Discovery and Validation of Novel LonP1 and Proteasome Inhibitor in IDH1-R132H Malignant Astrocytoma Models

Christopher Douglas[1], Naomi Lomeli[2], Javier Lepe[1], Kaijun Di[2], Nitesh Kumar Nandwana[3], Thao Vu[2], James Pham[2], Maria Cristina Kenney[3], Bhaskar Das[4,5]*, Daniela A. Bota[1,2,6]*

1 Department of Pathology & Laboratory Medicine, University of California Irvine, Irvine, CA, USA (C.D., D.A.B.)
2 Department of Neurology, University of California Irvine, Irvine, CA, USA (K.D., N.L., T.V., J.P.)
3 Department of Ophthalmology Research, University of California Irvine, Irvine, CA, USA (M.C.K.)
4 Arnold & Marie Schwartz College of Pharmacy & Health Sciences, Long Island University – Brooklyn, NY, USA (N.K.D, B.D.)
5 Department of Pharmacology, Long Island University – Brooklyn, NY, USA (B.D.)
6 Chao Family Comprehensive Cancer Center, University of California Irvine, Irvine, CA, USA (D.A.B.)

***Co-Corresponding Authors:** Daniela A. Bota, M.D., Ph.D.
University of California Irvine, Sprague Hall B200,
Irvine, CA 92697-4475, USA
Phone: (949) 824-7377
Fax: 714-456-6894
Email: dbota@hs.uci.edu

Bhaskar Das, Ph.D.
Long Island University – Brooklyn, 75 DeKalb Avenue, HS-610,
Brooklyn, NY 11201-5497
Phone: (718) 488-1471
Fax: 718-780-4586
E-mail: Bhaskar.Das@liu.edu

Funding: This work was supported by the National Institute of Neurologic Diseases and Stroke Award (NINDS/NIH) [NS109423] to DAB and BD. This work was also supported by the NINDS/NIH Award [NS111303], the National Center for Advancing Translational Sciences (NCATS/NIH) Award [UL1 TR001414], the UCI American Cancer Society Institutional Grant [ACS/IRG – 98-279- 07], the Ruth L. Kirschstein National Research Service T32 Award [2T32CA009054-41 (MPI)] and the UCI Cancer Center Award [P30CA062203] from the National Cancer Institute to DAB. *The content is solely the responsibility of the authors and does not necessarily represent the official views of the National Institutes of Health.*

Conflict of Interest: The authors have no conflicts of interest to disclose.

Authorship Statement: Conception and design of this work: DAB, BD, CD, KD, and NL. Inhibitor synthesis and design: BD and NKD. Brain mass spectrometry measurements: Cyprotex and Biotechnology Innovation and Optimization Center. Data collection, analysis, and interpretation: CD and DAB. All the authors critically reviewed and approved the final manuscript.

Manuscript Word Count: Abstract: 249; Importance of Study: 144; Text: 6103; References: 1777; Figure Legend: 551.

42 **Graphical Abstract**

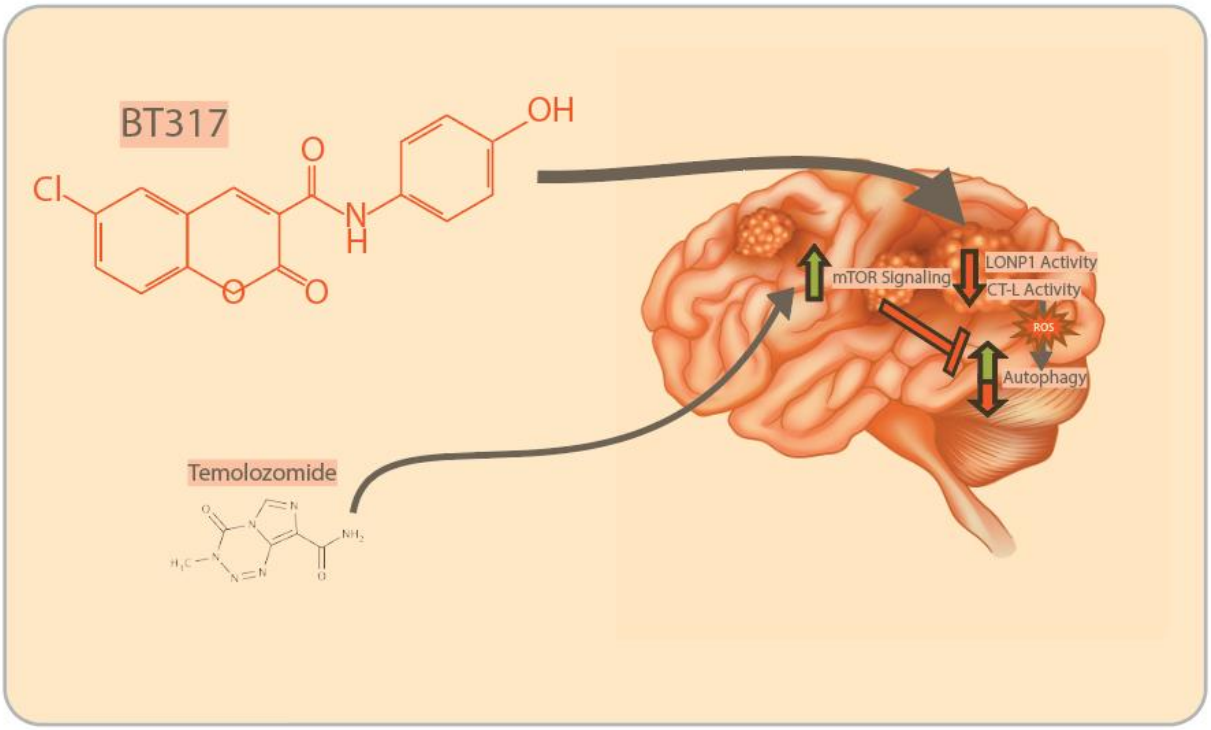

43

44 **Abstract**

45 Malignant astrocytomas are aggressive glioma tumors that have poor prognosis and limited treatments
46 available following recurrence. These tumors are characterized by extensive hypoxia-induced,
47 mitochondria-dependent changes such as glycolytic respiration, increased chymotrypsin-like (CT-L)
48 proteasome activity, decreased apoptosis, and increased invasiveness. Mitochondrial Lon Peptidase 1
49 (LonP1) is an ATP-dependent protease directly upregulated by hypoxia-inducible factor 1 alpha (HIF-1α).
50 Both LonP1 expression and CT-L proteasome activities are increased in gliomas and are associated with a
51 high tumor grade and poor patient survival. Recently, dual LonP1 and CT-L inhibition has been found to
52 exhibit synergy against multiple myeloma cancer lines.

53 We now report that dual LonP1 and CT-L inhibition has synergistic toxicity in IDH mutant astrocytoma
54 when compared to IDH wildtype glioma, due to increased reactive oxygen species (ROS) generation and
55 autophagy. A novel small molecule, BT317, was derived from coumarinic compound 4 (CC4) using
56 structure-activity modeling and was found to inhibit both LonP1 and CT-L proteasome activity and
57 subsequently induce ROS accumulation and autophagy-dependent cell death in high-grade IDH1 mutated
58 astrocytoma lines. *In vitro*, BT317 also had enhanced synergy with the commonly used chemotherapeutic
59 temozolomide (TMZ), which blocked BT317-induced autophagy. This novel dual inhibitor was selective to
60 the tumor microenvironment and demonstrated therapeutic efficacy both as a single agent and in
61 combination TMZ in IDH mutant astrocytoma models. We show that BT317, a dual LonP1, and CT-L
62 proteasome inhibitor exhibited promising anti-tumor activity and could be a promising candidate for
63 clinical translation in the space of IDH mutant malignant astrocytoma therapeutics.

64 Data Access Statement: Research data supporting this publication are as presented in the manuscript.

Keywords: IDH mutant astrocytoma, Glioblastoma, LonP1, CT-L proteosome, BT317

Highlights

1. The novel compound BT317 acts as a LonP1 and chymotrypsin-like proteasome inhibitor
2. LonP1 and CT-L proteasome inhibition drives ROS production in IDH mutant astrocytoma
3. LonP1 and CT-L proteasome inhibition drives autophagy in IDH mutant astrocytoma
4. BT317 shows blood-brain barrier permeability and has low normal tissue toxicity
5. BT317 synergizes with the first-line chemotherapy agent TMZ

Importance of Study

Malignant astrocytomas (IDH mutant astrocytomas grade 4 and IDH wildtype glioblastoma) have poor clinical outcomes, and novel treatments are needed to limit recurrence and improve overall survival. These tumors have a malignant phenotype that is mediated by altered mitochondrial metabolism and adaptation to hypoxia. Here, we present evidence that the small-molecule inhibitor BT317, with a dual Lon Peptidase 1 (LonP1) and chymotrypsin-like (CT-L) inhibition profile, can be effectively used to induce increased ROS production and autophagy-dependent cell death in clinically relevant, IDH mutant malignant astrocytoma, patient-derived orthotopic models. BT317 showed strong synergy with the standard of care, temozolomide (TMZ), in the IDH mutant astrocytoma models. This could lead to the development of dual LonP1 and CT-L proteasome inhibitors as novel therapeutic strategies for IDH mutant astrocytoma and provide insight for future clinical translation studies in combination with the standard of care.

1. Introduction

Malignant astrocytomas are one of the most aggressive primary and secondary brain tumors, with a three-year expected survival rate following surgical resection, radiation, and chemotherapy. Recurrence is certain after the initial treatment, and there is currently no proven therapy to significantly prolong survival after tumor recurrence[1,2]. The current standard of care, temozolomide (TMZ, temodar), an alkylating agent, provides a median survival advantage of 2.5 months when added to surgery and radiation therapy[3]. The use of Tumor-Treating Fields (TTFields, Optune) further increases this survival advantage by 4 months[4]. Despite significant efforts and numerous past and ongoing clinical trials utilizing small molecule inhibitors such as the STAT3 inhibitor WP1066, EGFR inhibitors, Dopamine Receptor D2 antagonists (ONC201), and new immunotherapy checkpoint inhibitor approaches such as pembrolizumab, nivolumab and ipilimumab, the development of safe and efficacious therapies for malignant astrocytomas has been slow. In the past 16 years, only three therapies (TMZ, bevacizumab, TTFields) have been approved for the treatment of astrocytomas[5]. Thus, there is an urgent need to develop alternative therapeutic strategies.

Malignant astrocytomas are increasingly classified based on their genetic and epigenetic profiles[6]. Less than 10% of grade 4 astrocytomas express isocitrate dehydrogenase 1 or 2 (IDH1/2) mutations, which are associated with an improved response to treatment and prognosis as compared with the IDH wildtype tumors[7]. Based on these biologic and survival differences, the most recent WHO glioma classification excludes tumors with an IDH mutation from being classified as GBM and refers to such tumors as astrocytoma grade 4, IDH mutant[8]. Even though the presence of the IDH mutations predict a better

103 outcome, the survival of patients with grade 4 IDH mutated astrocytoma treated with the standard
104 therapy (radiation and TMZ) is still only 31 months[9]. The presence of the IDH mutation (>90% are IDH1-
105 R132H) can drive tumorigenesis[10] at the cost of impairing the mitochondrial electron transport chain in
106 cellular mitochondria, increasing ROS production, and creating increased vulnerability to pro-oxidative
107 and apoptotic signals[11]. Direct targeting of the IDH1 mutation using specific inhibitors has proven
108 successful in other malignancies, notably IDH1-mutant Acute myelogenous leukemia, but had limited
109 results in IDH1 mutant malignant astrocytoma, and there is a great need to develop more targeted
110 strategies for this tumor type.

111 The invasive phenotype of malignant astrocytomas is partly mediated by overexpression of the
112 transcriptional activator hypoxia-inducible factor 1 alpha (HIF-1α). HIF-1α contributes to the hypoxia-
113 driven maintenance of glioma stem cells (GSCs)[12] by supporting self-renewal[13], angiogenesis[14], increased
114 invasiveness[15], and high levels of genetic instability. The latter contributes to tumor heterogeneity and
115 presents a major challenge in devising novel therapeutic strategies for its treatment[16]. There are hundreds
116 of gene targets in the HIF-1α signaling pathway and the nuclear-encoded Lon Peptidase 1 (LonP1) is
117 directly upregulated by HIF-1α[17]. LonP1 is an ATP-dependent protease that regulates mitochondrial
118 homeostasis through three main functions: (1) proteolytic degradation of mitochondrial proteins[17], (2)
119 protein chaperone[18], and (3) mitochondrial DNA (mtDNA)-binding protein[19]. LonP1 overexpression is a
120 poor prognostic factor that promotes invasion and metastasis in multiple cancers, including colorectal[20],
121 melanoma[20] and oral cancer[21]. Our previous results showed that LonP1 is overexpressed in astrocytomas
122 and its elevated expression levels are associated with high tumor grade and poor survival[22]. Furthermore,
123 LonP1 knockdown in established human glioma lines, D-54 MG and U-251 MG, reduced cell viability under
124 normal conditions, and drastically impaired survival under hypoxic conditions[22]. This is concomitant with
125 a decrease in mitochondrial respiration. Notably, LonP1 pharmacological inhibition using the coumarinic
126 compound 4 (CC4)[23] inhibited glioma cell proliferation and synergistically enhanced the therapeutic
127 efficacy of TMZ, *in vitro*[22].

128 There is difficulty in the generation of specific LonP1 inhibitors[23], which is attributable to its structural
129 similarities with other known proteases and the proteasome[24]. Most LonP1 inhibitors exhibit dual
130 inhibition of LonP1 and the proteasome[23]. Targeting specifically the chymotrypsin-like (CT-L) proteasome
131 activity may be beneficial, as it plays an important role in tumor cell survival[25] and treatment resistance[26].
132 Dual inhibition of LonP1 and the CT-L proteasome activity could be potentially beneficial as it could offer
133 additional therapeutic benefits compared with targeting either protease activity alone. Recent work in
134 multiple myeloma has demonstrated the strong synergy with LonP1 and CT-L proteasome inhibition[27],
135 using specific inhibitors previously shown to have no cross activity, and to target only LonP1, Bardoxolone
136 methyl (CDDO-ME)[28,29], and the CT-L proteasome activity, carfilzomib (CFZ)[30]. Bortezomib (BTZ) exhibits
137 dual LonP1 and CT-L inhibition and possesses a boronic acid group that can transform into a boronate
138 ester when exposed to reactive oxygen species (ROS)[31]; however, it has poor blood-brain barrier (BBB)
139 permeability[32]. In the subcutaneous U-87 MG and U-251 MG glioma models, BTZ was found to sensitize
140 the glioma tumors to TMZ by suppressing FOXM1-mediated treatment resistance[33]. This study did not use
141 patient-derived lines and resorted to using a subcutaneous model instead of an orthotopic xenograft
142 model. In this study, we present BT317, a derivative of CC4[22,23] and a dual LonP1 and CT-L inhibitor. We
143 assessed its LonP1 protease and proteasome inhibition profiles. We then investigated the efficacy and
144 feasibility of the lead compound BT317 as a single agent and in combination with TMZ as a therapeutic

145 strategy for specifically IDH mutated malignant astrocytomas, including in two separate IDH1-R132H
146 patient-derived, orthotopic xenograft models.

147 **2. Methods**

148 ***2.1. Ethics Statement***

149 All astrocytoma tumor specimens were collected under institutional review board approved protocols
150 from patients who underwent surgical tumor resection at the University of California Irvine Medical
151 Center. The neuropathological review was completed by a specialized neuropathologist. All patient-
152 derived samples were deidentified. All animal studies were performed in accordance with the guidelines
153 established by the Institutional Animal Care and Use Committee (IACUC) at the University of California
154 Irvine.

155 ***2.2. Synthesis of small molecule BT317 and related compounds***

156 Synthesis of BT317 was initiated using compound **D** (methyl 6-chloro-2-oxo-2H-chromene-3-carboxylate)
157 (**Fig. 1A**). Compound **D** was then synthesized from Compound **A** using the outlined process by first adding
158 5-chlorosalicyclaldehyde (A, 1.55 g, 10 mM) to CH_3CN (5 mL) in a 35 mL reaction tube. Dimethylmalonate
159 (**B**) (1.45 g, 11 mM) and ethyl piperdine-3-carboxylate (**C**) (15 mg, 10 mol%) in 15 mL of CH_3CN were added.
160 The resulting reaction mixture was stirred at room temperature for 24 h. After the evaporation of CH_3CN,
161 the crude reaction mixture was purified by silica gel chromatography to give a white solid **D** (1.6 g, 60%).
162 Basic hydrolysis of compound **D** was performed to produce Compound **E** acid (6-chloro-2-oxo-2H-
163 chromene-3-carboxylic acid). Acid synthesis was initiated by adding methyl 6-chloro-2-oxo-2H-chromene-
164 3-carboxylate D (1.0 g, 4.2 mM) in ethanol to sodium hydroxide (10% w/v in 20 mL ethanol). The mixture
165 was stirred under reflux for 24 h. After the completion of the reaction, the mixture was cooled to room
166 temperature and diluted with 10% HCl. The solid precipitated out and was isolated and washed with
167 water, yielding compound **E** (white solid, 80% yield). Using compound **E**, we further derivatized to amide
168 (BT173) using a simple amide coupling reaction in the presence of coupling reagents. The 6-chloro-2-oxo-
169 2H-chromene-3-carboxylic acid **E** (1.0 mM) was dissolved in dichloromethane (DCM) (3 mL) in a 35 mL
170 reaction tube. Then 4-hydroxy aniline (1.1 mM) and DCC (1.2 mM) were added. The resulting reaction
171 mixture was stirred at room temperature for 24 h. The reaction was then quenched with a saturated
172 aqueous NaOH solution and extracted with DCM (10 × 3 mL). The combined organic layers were dried
173 over Na_2SO_4 and then filtered. After evaporation of the organic solvent, the residue was purified by silica
174 gel chromatography to obtain BT317, 6-Chloro-N-(4-hydroxyphenyl)-2-oxo-2H-chromene-3-carboxamide
175 (**Fig. 1B;** white solid, 78% yield). The reagents used for the synthesis were purchased from Fisher Scientific.
176 The structure was confirmed by nuclear magnetic resonance (NMR) and proton, carbon, and mass
177 spectrometry, and the purity of the compound was determined by HPLC. The lead compound, BT317, was
178 evaluated using NMR as follows: 1H NMR (500 MHz, DMSO-d6) δ 10.44 (s, 1H), 9.43 (s, 1H), 8.87 (s, 1H),
179 8.16 (d, J = 2.5 Hz, 1H), 7.82 (dd, J = 8.8, 2.6 Hz, 1H), 7.61 (d, J = 8.9 Hz, 1H), 7.53 (d, J = 8.5 Hz, 2H), 6.78
180 (d, J = 8.4 Hz, 2H). 13C NMR (125 MHz, DMSO) δ 160.0, 158.8, 154.2, 152.4, 145.7, 134.2, 133.5, 129.5,
181 129.0, 121.6, 121.2, 119.9, 118.2, 115.3. HRMS (ESI) was calculated for $C_{16}H_{11}ClNO_4$ (M.W. = 316.0371)
182 and 316.0607 [M + H]+.

183

184 ***2.3. Primary and Established Cell Lines***

185 *Primary Glioma/Astrocytoma Stem Cell Cultures (GSC)*

186 Patient-derived GSC were isolated from surgical astrocytoma samples in the laboratory of Dr. Daniela A.
187 Bota (DAB), using a previously established method[34]. All GSC cultures were maintained as non-adherent
188 neurospheres in Neurobasal medium (Thermo Fisher; 12349015) supplemented with 20 µg/mL EGF
189 (Thermo Fisher; PHG0313), 20 µg/mL FGF (Thermo Fisher; PHG0023), B27 (Life Technologies; 12587010),
190 GlutaMAX (Thermo Fisher; 35050061), 5 mM sodium pyruvate (Thermo Fisher; 11360070), and antibiotics
191 (Thermo Fisher; 15070063, 15290018). The patient-derived GSC lines included DB70, DB76, DB77, DB81,
192 and 83MES. The patient-derived 83MES line was a kind gift from Dr. Ichiro Nakano at the University of
193 Alabama at Birmingham.

194 *Established Human Glioma Cell Lines*

195 Five established human glioma cell lines, U-251 MG, D-54 MG, and U-87 MG, and the pediatric CHLA-200,
196 were maintained in DMEM/F-12 medium (Corning; 10-090-CV) containing 292 µg/ml glutamine, 1%
197 penicillin/streptomycin (Thermo Fisher; 15070063), and 10% FBS (Invitrogen; 10371-029). All the cell
198 cultures were maintained at 37°C and 5% CO_2 in a humidified incubator.

199 *Normal Cell Lines*

200 The human mammary gland epithelial adherent non-tumorigenic cell line MCF-10A was maintained in
201 DMEM/F-12 medium containing 0.5 mg/mL hydrocortisone, 20 ng/mL hEGF, 100 ng/mL cholera toxin, 1%
202 penicillin/streptomycin, and 5% horse serum (Life Technologies; 26050-070). The human lung fibroblast
203 line HPF242 was maintained in DMEM/F-12 containing 10% FBS and 1% penicillin/streptomycin. All the
204 cell cultures were maintained at 37°C and 5% CO_2 in a humidified incubator. Unlisted reagents were
205 purchased from Sigma-Aldrich and Thermo Fisher Scientific.

206 ***2.4. XTT Viability Assay***

207 All established and patient-derived astrocytoma cell lines were seeded at a density of 10,000 cells per well
208 in a 96-well plate (n = 4 replicates per condition). The following day, equal volumes of synthesized
209 inhibitors dissolved in DMSO were added to each well at the specified concentrations (0.1-1000 µM). For
210 the synergy experiments, BT317 was added at specified concentrations with a fixed and specified TMZ
211 concentration. After 72 h, 100 µL volume was removed from each well, and 75 µL of a pre-filtered solution
212 of 1 mg/mL XTT sodium salt (Alfa Aesar, 111072-31-2) and 20 µL/mL XTT activator (Trevigen, 4891-025-
213 02) dissolved in PBS (pH 7.4; Gibco; 10010-023) was added. After 4 h, the absorbance was measured at
214 490 nm using a SpectraMax Plus 384 microplate reader. GraphPad was then used to perform a log
215 transformation and generate a nonlinear regression curve to calculate IC_{50} viability. The Biochemically
216 Intuitive Generalized Loewe Model (BIGL) was used to determine agonism or antagonism (https://cran.r-
217 project.org/web/packages/BIGL)[35].

218 ***2.5. Reactive Oxygen Species Assay***

219 The DB70 line was plated and incubated for 12 h prior to starting treatment. CellROX™ Orange Reagent
220 (Thermo Fisher, C10443) was then added at a working concentration of 5 µM for 30 minutes. After several
221 1X PBS washes, the cell samples were replated and then imaged using a 20X objective on a Keyence BZ-
222 X810 Widefield Microscope.

223 ***2.6. Colony Forming Assay***

224 The DB70 line was treated for 24 h, then plated on 24-well PDL-coated plates for 10 days with partial
225 medium changes at days 4 and 7. Samples were fixed on day 10 with 4% paraformaldehyde for 30 minutes
226 prior to labeling with DAPI in 0.3% Triton 1X PBS. After additional 1X PBS washes, the plates were imaged
227 using a 4X objective on a Keyence BZ-X810 Widefield Microscope.

228 ***2.7. Western Blotting***

229 Cell culture samples were exposed to BT317 for 1, 4, 8, and 72 h prior to lysis with RIPA lysis buffer
230 containing 1 mM PMSF, 1 mM Na_3VO_4, and a protease inhibitor cocktail (Sigma, P8340-1ML). The protein
231 concentration was standardized using the DC Protein Assay (Bio-Rad, 500-0114) with a SpectraMax Plus
232 384 microplate reader. A Precision Plus Protein Kaleidoscope™ ladder (Bio-Rad, 161-0375) and
233 approximately 20 µg of sample were loaded onto each well and run on a Mini Protean TGX Gel (Bio-Rad,
234 456-1046) before being transferred to an Immobilon Transfer Membrane (Millipore, IPVH08130). The
235 membranes were probed with the indicated primary antibodies and the appropriate secondary
236 antibodies. The primary and secondary antibodies used were 1:2000 LonP1 (Proteintech, 15440-1-AP),
237 1:1000 Aconitase2 (Abcam, ab71440), 1:1000 LC3B (Cell Signaling Technology, 2775S), FOXM1 (Millipore
238 Sigma, SAB1412254-100UG), C-MET (Fisher Scientific, MAB3729), TFAM (Fisher Scientific, PA5-80107)
239 1:2000 B-Actin (Novus Biologicals, NB600-501), 1:1000 p-AKT (Abcam, ab192623-100ul), 1:10,000 goat
240 anti-mouse IgG F(ab')2 (Enzo Life Sciences, ADI-SAB-100-J), and 1:3,000 IgG (H+L) Goat anti-Rabbit HRP
241 (Invitrogen, 32460); these were used according to the manufacturer's recommendations and diluted in
242 TBST with 3% BSA. Chemiluminescence was visualized using Amersham™ ECL™ Prime western blotting
243 Detection Reagent (GE Healthcare, RPN2232) and imaged using an Azure c600 Molecular Imager. ImageJ
244 was used to align the bands, improve contrast (<20%), and normalize and quantify all bands.

245 ***2.8. LonP1 Protease Activity Assay***

246 The total proteolytic activity of purified recombinant LonP1 (Abcam, ab160451) was analyzed using a
247 Pierce Fluorescent Protease Assay Kit (Thermo Scientific™, 23266). A mixture of 200 nM LonP1 and 10
248 mM $MgCl_2$ was prepared in BupH™ Tris-buffered saline. LonP1 inhibitors or vehicle (DMSO) were then
249 added, and the samples were incubated at 37°C for 1 h. Following this incubation, an equal volume of 0.04
250 mg/mL FITC-casein (Thermo Scientific™, 23267), 4 mM ATP (Thermo Fisher, R0441), and 10 mM $MgCl_2$
251 was added prior to measurement using a Biotek Synergy HT plate reader. Digestion of fluorescein-labeled
252 casein was assessed by measuring fluorescence with excitation and emission filters at 490 and 525 nm,
253 respectively.

254 ***2.9. Proteasome Activity Assay***

255 Proteolytic activity was assessed using a Proteasome-Glo™ assay system (Promega, G8531), comprising
256 Proteasome-Glo™ Chymotrypsin-Like Assay (G8621), Proteasome-Glo™ Trypsin-Like Assay (G8621) and
257 Proteasome-Glo™ Caspase-Like Assay (G8621). The assay was performed according to the manufacturer's
258 instructions. Tissue samples were flash frozen and ground using a Dounce Homogenizer (Fisher, 50-194-
259 5205). Samples were then harvested in ice-cold lysis buffer composed of 50 mM HEPES (pH 7.4), 250 mM
260 sucrose, 5 mM $MgCl_2$, 0.5 mM DTT, and 40 mM KCl in deionized, sterile water. For D-54 MG, cells were
261 seeded at a density of 200,000 cells per well onto a 6-well plate and subsequently exposed to LonP1
262 inhibitors (BT317, BT395, BT397, and BT399) at the specified concentrations and endpoints. The lysates
263 were incubated on ice for 30 min and centrifuged at 14,000 rpm for 10 min at 4°C. The supernatants were
264 collected and mixed 1:1 with stabilizing buffer composed of 40 mM HEPES (pH 8.0), 1 mM EDTA, and 20%

265 glycerol in deionized, sterile water. The protein concentration was standardized using the DC Protein
266 Assay (Bio-Rad, 500-0114) with a SpectraMax Plus 384 microplate reader. Samples were then diluted with
267 ice-cold proteasome dilution buffer and plated in a black, clear, flat-bottom 96-well plate at a
268 concentration of 8 µg protein in 50 µL/well (n = 3-4 replicates/sample). The plates were placed on a plate
269 shaker at 300-500 rpm for 30 s, followed by incubation for 10-30 minutes incubation at room temperature.
270 Luminescence was read using a Biotek Synergy HT plate reader.

271 ***2.10. BT317 and TMZ Administration and Maximum Tolerated Dose (MTD) Escalation***

272 BT317 and TMZ was reconstituted in DMSO to create a concentrated stock prior to further dilution in 500
273 µL 1XPBS to generate the correct dosage for intraperitoneal injection (i.p.) in 10-14 week-old Rag1 KO
274 immunodeficient mice (Jackson Laboratory, B6.129S7-*Rag1*^{tm1Mom}/J). Mice were monitored following
275 injection and the clinical score was determined based on activity, appearance, and body condition with a
276 maximum score of 3, which is necessary to define the MTD[36]. Mass spectrometry was performed on flash-
277 frozen brains and tail vein blood draws by contract research organizations (Cyprotex and Biotechnology
278 Innovation and Optimization Center) to determine BT317 levels.

279 ***2.11. Patient-derived Orthotopic Xenograft Model***

280 The patient-derived lines DB70, DB76, DB77 and 83MES were seeded into 3-dimensional organoids using
281 an established methodology[37]. Upon full expansion, the organoids were dissociated, and 1,000-10,000
282 cells were intracranially implanted into the right frontal lobe of 10-14 week-old Rag1 KO immunodeficient
283 mice (Jackson Laboratory, B6.129S7-*Rag1*^{tm1Mom}/J). After 5 or 10 days, treatment was initiated as specified,
284 with intraperitoneal (i.p.) injections every other day for a total of 5 doses over a span of 5 or 10 days as
285 specified. Animals were observed daily and sacrificed upon observation of distress, including hemiparesis,
286 obtundation, hunchback, or weight loss of 20% from the maximum weight achieved.

287 ***2.12. Statistical Analysis***

288 Data were analyzed using Student's *t*-test or log-rank (Mantel-Cox) test when appropriate. Data are
289 presented as mean ± standard error of the mean (SEM). Significance between groups is denoted by $^{*}P$
290 <0.05, $^{**}P<0.01$, $^{***}P<0.001$. Data were analyzed using the GraphPad Prism 5.0 software (GraphPad
291 Software, La Jolla, CA, USA). For the XTT viability assays, raw data were processed using a log transform
292 and a dose-response inhibition nonlinear model to determine IC50 and standard error. The statistical
293 significance of the Kaplan-Meier survival curve was verified using the Mantel-Cox log-rank test.

294

295 **Results**

296 **3.1 Dual LonP1 and Chymotrypsin-like Activity Exhibits Enhanced Synergy on IDH1 Mutant Malignant**
297 **Astrocytoma Patient Derived Lines and Induces Greater Autophagy as Compared with IDH Wildtype**
298 **Lines.**

299 Previous findings suggested that dual LonP1 and chymotrypsin-like (CT-L) proteasome inhibition may be
300 an effective strategy for targeting cancer cells; however, the exact mechanism has not been validated.
301 Here, we demonstrated that the selective LonP1 inhibitor, CDDO-ME[28], and CT-L proteasome inhibitor,
302 Carfilzomib (CFZ)[28,29], have strong synergy in reducing viability of multiple patient-derived malignant
303 astrocytoma lines (**Fig. 1A**). Interestingly, the IDH1-mutant astrocytoma patient-derived lines DB70 and

304 DB76 are sensitive to CDDO-ME doses as low as 200 nM CDDO-ME with CFZ at 1 and 5 nM; however, this
305 combination has more limited activity against IDH wildtype DB77 and 83MES lines (e.g., >400 nM CDDO-
306 ME, **Fig. 1B**). In the DB70 line, CDDO-ME treatment (200 nM) increased levels of the autophagy marker,
307 LC3B-I[38] , which is further increased by 3, 8, 1.5-fold with co-incubation of 5 nM CFZ at 1, 12 and 24 h,
308 respectively. In DB76, a 13, 1.5, 3-fold increase was observed in LC3B-I at 1, 12 and 24 h, respectively. CFZ
309 alone did not alter LC3B-I levels (**Fig. 1C**). Furthermore, a significant increase in reactive oxygen species
310 (by ~50%) is observed after 12 h of 200 nM CDDO-ME and 5 nM CFZ treatment (**Fig. 1D**) as opposed to
311 either CFZ or CDDO-ME separately. However, none of the aforementioned treatments resulted in an
312 increase in ROS in the 83MES line.

313

314 ***3.2. Structure Activity Relationship Modeling for Developing CC4 Derivatives.***

315 Our previous work with CC4 demonstrated that LonP1 inhibition could inhibit astrocytoma cell growth,
316 adaptation to hypoxic conditions, and increase the anti-tumor efficacy of TMZ[22]. Coumarinic compounds
317 have been found to exhibit high hepatotoxicity[39]. To decrease off-target toxicity and improve anti-tumor
318 efficacy, we derived four novel LonP1 inhibitors from CC4 using structure-activity relationship (SAR)
319 modeling. A library of small molecules (e.g., BT395, BT397, BT399, and BT317) was identified *in silico,*
320 using customized computational protein structure modeling programs M4T, MMM, Mutate, and SAR with
321 Autodock4, Surflex-Dock, ICM, PESD, and SFC (B. Das, unpublished data). The CC4 ester group was
322 modified to develop peptidomimetic compounds (amides and oxadiazoles) with increased water
323 solubility. As a part of our rational design study, rings **A**, **B** and **C** were modified (**Fig. 2A**). Finally, the
324 hydrophobic portion of rings **A** and **B** was replaced with quinolinolin-2 (1H)-1 to improve solubility (**Fig.
325 2B**; BT317). We developed also developed a library of additional CC4 derivatives; as shown in
326 **Supplementary Fig. 2**. In Ring **A**, the benzyl group is prone to oxidation *in vivo* by oxidative cytochrome
327 enzymes to form acidic chloride, which is associated with high toxicity. Therefore, chlorine was directly
328 substituted at position 6 of the ring. The hydroxyl group on ring **C** was converted to a boronic ester group.
329 The boronic acid and potassium salts of trifluoroborate and acid isosteres are known to increase cell
330 permeability and reduce toxicity[40]. Furthermore, boronic acid and ester-based prodrugs were used as
331 templates for ring **C** because boronic acid is selective for H_2O_2[31].

332

333 ***3.3. Novel CC4 Derivative, BT317, Exhibits On-Target Inhibition of LonP1 Protease and Proteasome
334 Activity***

335 Using our structure-activity relationship modeling approach, we derived BT317, BT395, BT397 and BT399
336 from CC4 and evaluated their relative LonP1 and proteasome inhibition profiles. To evaluate the on-target
337 inhibition potency of these compounds, we assessed LonP1 protease activity inhibition using a FITC-casein
338 assay (**Fig. 3A and Supplementary Fig. 3A**). BT317 demonstrated LonP1 protease inhibition with an IC_{50}=56
339 µM, while BT397 exhibited similar inhibition with an IC_{50}=58 µM. The other inhibitors showed no inhibition
340 of LonP1 protease activity (data not shown). Since most LonP1 inhibitors exhibit dual inhibition of LonP1
341 and proteasome[23], we next examined whether the compounds also inhibit the 20S proteasome. For this
342 assay, we prepared extracts from the established malignant glioma cell line, D-54 MG (**Fig. 3B**). At 10 µM,
343 BT317 yielded a ~98 and 96% reduction in CT-L activity, a ~26% and 27% reduction in trypsin-like (T-L)
344 activity, and a ~23% and 30% reduction in caspase-like (C-L) activity at both 1 and 4 h, respectively. The

345 proteasomal activity of all three complexes returned to baseline at 8 h post-treatment. The BT395, BT397
346 and BT399 compounds showed limited inhibition of proteasome activity (**Supplementary Fig. 3C**). The
347 antioxidant N-acetyl cysteine (NAC) inhibits the production of ROS and is a known blocker of proteasome
348 inhibitors[41]. BT317 proteasome inhibition was eliminated by 10 mM NAC co-treatment.

349 In contrast to the other tested compounds, BT317 demonstrated quicker kinetic inhibition of CT-L
350 proteasome activity than BTZ (**Fig. 3B**), which is a potent dual LonP1 and CT-L proteasome inhibitor
351 approved for the treatment of multiple myeloma[42]. The observed CT-L inhibition by BTZ demonstrates
352 limited inhibition by comparison to BT317. Given the potent on-target LonP1 protease inhibition of BT317
353 and its accelerated CT-L proteasome inhibition, we selected BT317 for further evaluation as a dual
354 LonP1/proteasome targeted therapy in our astrocytoma models.

355 The mitochondrial matrix protein aconitase (Aco2) is the most important protease substrate for LonP1[43].
356 To evaluate the effect of BT317 on LonP1 substrate levels, we treated the established IDH wildtype D-54
357 MG and U-87 MG glioma lines with 10 µM BT317, well below the expected LonP1 protease inhibition
358 concentration, IC_{50} = 56.03 µM (**Fig. 3C**). The D-54 MG line responded with a pronounced Aco2 protein
359 level increase of 2-fold at 1 h; however, this was quickly reversed by 8 and 24 h. TFAM was still elevated
360 by 3-fold at 24 h. We also compared this result with 100 nM Bortezomib (BTZ), a dual LonP1[30] and CT-L
361 proteasome inhibitor. In the D-54 MG line, BTZ resulted in decreases in Aco2 levels at 24 h to 0.3-fold;
362 however, it increased TFAM levels by 4-fold. In the U-87 line, BT317 resulted in the accumulation of Aco2
363 gradually to 3-fold and TFAM accumulated by 1.5-fold after 24 h and this effect was similarly mimicked by
364 BTZ with 2.4 and 2.1-fold increase in protein levels, respectively. The LonP1 substrate
365 accumulation/degradation observed exceeded what was expected given that previously demonstrated
366 LonP1 protease inhibition.

367

368 ***3.4. BT317 Exhibits Synergy with Temozolomide in Autophagy-Dependent Cell Death in IDH1 Mutant***
369 ***Malignant Astrocytoma***

370 Current glioma research and clinical trials emphasize the role of GSCs in tumor maintenance, resistance
371 to therapies, and local invasion[44]. The patient-derived lines are enriched for tumor-initiating cancer stem
372 cells by passaging in serum-free, suspension culture with referenced growth factors and have been shown
373 to recapitulate the expression profile of the original patient sample[45]. Using the XTT assay, we determined
374 the IC_{50} viability of established and patient-derived GSC lines in response to 72 h of exposure to BT317 at
375 graded doses (**Fig. 4A panel 1**). BT317 had increased toxicity towards the patient-derived GSC lines (i.e.,
376 83MES, DB70, DB76, DB77, DB81; **Supplemental Table 1**) as compared to the established and
377 differentiated astrocytoma lines, consistent with previous research which demonstrated that GSC are
378 more sensitive to proteosome and LonP1 inhibition as compared with the more differentiated established
379 lines[46]. The sensitivity of the DB70 line did not differ significantly from the DB81 line, derived from the
380 same patient following recurrence. BT317 also showed less activity towards the CHLA-200 pediatric line
381 (IC_{50}=73.61 µM). The normal cell lines, HPF242 and MCF10A, fibroblasts, and human astrocytes, also
382 exhibited higher viability following treatment with BT317. Furthermore, BT317 synergized with 10 µM
383 TMZ to decrease cell viability in the TMZ-resistant DB70 and DB76 GSC lines (recurrence following TMZ
384 treatment) (**Fig. 4A panel 2, and S4A**). Interestingly, this synergy was not observed in the IDH wildtype
385 lines (**Fig. 4A panel 3 and S4A**). Co-incubation of 10 µM BT317 with 10 µM TMZ in the DB70 line resulted
386 in a significant increase in ROS by 1.5-fold (**Fig. 4B**). BT317 alone did induce a significant increase in ROS

387 by 1.3-fold at 8 h in the DB70 line; however, a slight decrease in ROS to 0.78-fold was observed at 4 h
388 following treatment in the 83MES line (**Supplementary Fig. 4C**). The IDH1 mutant lines exhibited increased
389 LC3B-I and II at 1, 12, 24 h post-treatment and this was reversed with co-incubation with 10 µM TMZ.
390 Furthermore, C-MET and FOXM1 levels increased with BT317 or TMZ alone; however, the combination
391 resulted in a decrease in C-MET and FOXM1 levels. This also coincided with a significant increase in Aco2
392 and TFAM with or without TMZ. The mTOR pathway (e.g., pAKT), which is capable of suppressing
393 autophagy, was also upregulated with TMZ incubation at the earlier timepoints in the DB70 line; however,
394 this was less obvious in the DB76 line, where there was a change of 0.57 and 1.83-fold for both bands at
395 1 h after combinatorial treatment (**Fig. 4C**). In the IDH1 wildtype lines, BT317 also increased LC3B-I, Aco2
396 and TFAM levels. DB77 showed minimal increase in LC3B-I levels by 1.43-fold that was reduced to 0.44-
397 fold by 24 h, while 83MES did not show ablation of autophagy induced by co-incubation with TMZ.
398 Interestingly, this appeared to correspond with a decrease in pAKT levels with co-treatment of BT317 and
399 TMZ. In contrast, the DB77 line did exhibit elevated pAKT at 1 with co-treatment and 24 h with TMZ alone
400 (**Fig. 4C and S4B**) The more modest increase in pAKT following TMZ treatment could be due in part to the
401 increased resistance to TMZ alone exhibited by the DB76 and DB77 lines – particularly at 10µM TMZ. In
402 the IDH mutant DB76 line, the large autophagic response with BT317 treatment may partly explain its
403 sensitivity to modest activation of mTOR signaling with TMZ treatment (**Supplementary Fig. 4D**). This
404 muted autophagic response highlights the limited autophagy-induced cell death at 25uM BT317 in the
405 DB77 line and the lack of autophagy-dependent cell death in the 83MES line, following co-incubation with
406 3mM 3-methyladenine (3-MA), an autophagy inhibitor. As expected in the IDH1 mutant lines, autophagy-
407 dependent cell death was evident at lower concentrations of BT317; however, this was not observed for
408 the IDH wildtype lines (**Fig. 4D**). Furthermore, the combinatorial treatment resulted in overall lower levels
409 of FOXM1 at the 24 h timepoint for DB70, DB76 and 83MES at ~0.5, 0.5 and 0.3-fold decreases,
410 respectively. This mimics previous observations with the combinatorial treatment of BTZ and TMZ[33]. DB77
411 showed a relative increase of ~0.2-fold. It was previously reported that TMZ targets more differentiated
412 populations with an average IC_{50} of ~540 µM against similar glioma lines[47], whereas BT317 offers far
413 greater efficacy against the harder to eradicate GSC populations (**Supplementary Table 1**). This further
414 highlights the potential use of BT317 in combination with TMZ as a treatment modality to target diverse
415 cell populations and potentially to reverse malignant astrocytoma treatment resistance.

416

417 ***3.5. BT317 Exhibits Low Toxicity and its Activity is Localized to the Tumor Microenvironment***

418 Previous development of proteasome inhibitors for the treatment of GBM was limited by either poor BBB
419 penetrance (i.e., BTZ)[31] or by the presence of the central nervous system (i.e., MRZ= marizomib, confusion,
420 ataxia)[48] or peripheral nervous system (BTZ, peripheral neuropathy)[49] toxicity. The development of these
421 toxicities is directly related to the level of proteasome inhibition in the blood and in the normal brain[50].

422 Prior to evaluating efficacy, we established the maximum tolerated dose (MTD). Using a previously
423 established methodology[36], we observed the clinical score following treatment (n=2) with iterative 50%
424 dose escalation until we determined the MTD to be >180 mg/kg (data not shown). We repeated a
425 continuous dose series over 10 days with 100 mg/kg of BT317 every other day or daily. There was no
426 noticeable drop in weight or any observable clinical signs (**Fig. 5A**). Next, we administered 100 mg/kg
427 BT317 and 25 mg/kg TMZ or 100 mg/kg BT317 and 50 mg/kg TMZ daily for 10 days. A temporary drop in
428 weight and minor clinical signs were observed following the first 2 doses with 100 mg/kg BT317 and 50

429 mg/kg TMZ; however, the animal weight normalized by day 4 and no further clinical signs were observed.
430 Novel therapeutic candidates for malignant astrocytomas must have superior BBB penetrance, target
431 GSCs, synergize with the standard of care, TMZ, and demonstrate improved survival *in vivo*. To assess BBB
432 penetrance, 9x BALB/c mice received a single intraperitoneal (i.p.) injection of BT317 (3 mg/kg). The
433 animals were euthanized 30, 60, and 120 min post-BT317 injection (n=3 per endpoint). Brain and plasma
434 samples were collected, and BT317 (ng/mL) levels were quantified using mass spectrometry (**Fig. S5A**).
435 BT317 levels reached ~390 ng/mL in the brain at 30 min and decreased to ~55 ng/mL at 120 min post-
436 injection. At all measured endpoints, levels in the brain were significantly higher than those in the plasma.

437 To evaluate the on-site activity of BT317, we performed an intracranial implantation with the DB70 line
438 and after 15 days administered a single dose of 100 mg/kg of BT317 to the mice prior to analyzing
439 proteasome activity in the blood, healthy brain, and intracranial tumor mass (**Fig. 5B**). The animals were
440 euthanized 1 and 4 h post-injection (n=6 per endpoint). BT317 showed ~70% and 60% inhibition of CT-L
441 and C-L activity in the tumor, respectively, compared with ~50% and 25% for MRZ at 4 h. Only MRZ showed
442 CT-L inhibition in the normal healthy brain with a ~40% reduction at 1-4 h. Furthermore, MRZ also
443 inhibited CT-L, T-L, and C-L in the blood by ~90%, 35-45%, and 30%, respectively. BT317 did not inhibit
444 proteasome activity in the blood. Both BT317 and MRZ showed accumulation of Aco2 in the tumor at 4 h
445 with ~60-70% increase on average (**Supplementary Fig. 4**).

446

447 ***3.6. BT317 and Combinatorial Treatment with BT317 and TMZ Increases Survival***

448 Next, we assessed the efficacy in an orthotopic xenograft model using the GSC patient-derived, IDH1-
449 R132H DB70 and DB76 lines. Rag1 KO mice were intracranially implanted with DB70 or DB76 (1000
450 cells/mouse), dissociated from a novel *in vitro,* organoid model[37] (**Fig. 6**). A total of 5 doses were
451 administered at 100 mg/kg BT317 ± 50 mg/kg TMZ daily, starting 10 days after intracranial xenograft
452 implantation and continuing for a total of 5 days. BT317 alone significantly improved the median survival
453 by 1 ($p<0.05$) and 3 days ($p<0.05$) in the DB70 and DB76 xenografts, respectively. The combination of
454 BT317 and TMZ significantly improved overall survival ($p<0.01$); however, median survival for the
455 combinatorial cohorts could not be determined by the end of the experiment. We also found that earlier
456 dosing regimen starting on day 5 for a total 5 doses of 100 mg/kg BT317 every other day significantly
457 increased median survival from 25 to 33 days in the DB70 PDX model (10,000 cells/mouse, **Supplementary**
458 **Fig. 6A**). The 83MES PDX model also showed a modest increase in median overall survival from 17.5 to 19
459 days; however, this required an escalated dosage of 150 mg/kg BT317 (10,000 cells/mouse,
460 **Supplementary Fig. 6B**).

461

462 **Discussion and Conclusion**

463 Previously, we demonstrated that the LonP1 inhibitor, CC4, was effective against established glioma lines
464 and that proteosome inhibition with marizomib is effective in *in vitro* and *in vivo* glioma models, though
465 its clinical use is limited by significant CNS toxicity[51]. Here we have reported on the designing of the novel
466 LonP1 and CT-L proteosome inhibitor, BT317, which has specific activity and limited toxicity.

467 For our rational design and SAR modeling, we used customized computational protein structure modeling
468 programs, as well as standard programs, to identify the lead compounds that could be derived from CC4

469 to improve solubility and BBB permeability and reduce toxicity. For compound design, we used the Lipinski
470 rule of 5 with the following considerations: (1) biological activity (i.e., more sp3 carbon atoms), (2) ease
471 of synthesis, and (3) moderate compound complexity to minimize toxicity and off-target effects[52].

472 Our lead molecule, BT317, exhibited dual inhibition of LonP1 protease activity and CT-L proteasomal
473 activity, on-target LonP1 inhibition, BBB permeability, low animal toxicity, and prolonged survival with
474 and without the standard-of-care in two patient-derived IDH1-R132H GSC intracranial xenograft models.
475 BT317 accumulated at higher levels in the brain than in the plasma at 30 min post-administration. Its
476 potent dual inhibitory activity can be compared with that of BTZ, a potent proteasome inhibitor that also
477 inhibits LonP1 protease activity. However, BTZ has limited penetrance into the brain, and a phase II clinical
478 trial of BTZ and bevacizumab in recurrent GBM was hindered due to dose-limiting sensory neuropathy
479 associated with BTZ[53]. Another CT-L proteasome inhibitor tested for GBM was ritonavir. Nonetheless,
480 ritonavir failed to demonstrate efficacy due to the development of resistance, *in vivo*[54]. Marizomib has
481 also shown improved survival in orthotopic GBM models; however, it has exhibited underlying issues with
482 significant CNS toxicity (confusion, ataxia, fatigue)[55] in phase 2 studies and did not improve survival in a
483 phase 3 randomized clinical trial[48]. This toxicity is represented by the high rate of marizomib-treated
484 patients that have neurologic (67%) and psychiatric (52%) adverse events[51]. Additionally, the high MTD
485 and specific tumor activity of BT317 further demonstrate its potential as a less toxic dual LonP1 and
486 proteasomal inhibitor for GBM treatment.

487 GBM is characterized by mitochondrial dysfunction, including metabolic shifts towards aerobic glycolysis,
488 elevated ROS generation, and sensitivity to metabolic stress[22]. Aconitase participates in the tricarboxylic
489 acid cycle (TCA) by converting citrate to isocitrate; however, its involvement in malignant astrocytoma
490 metabolism is unclear. Recent studies have shown that Aco2 levels are decreased in breast cancer cell
491 lines and patient-derived tumor biopsies, and Aco2 overexpression impairs breast cancer cell proliferation
492 and mitigates the Warburg effect by redirecting pyruvate to the mitochondria[56]. In addition to its role in
493 the TCA cycle, aconitase also promotes mtDNA stability by interacting with nucleoids (protein-mtDNA
494 complexes)[57]. Our findings revealed pronounced Aco2 accumulation in stable GBM lines and patient-
495 derived GSCs following BT317 exposure. Notably, BT317 induced Aco2 accumulation at 10 µM despite the
496 IC_{50}=56 µM for LonP1 protease inhibition. This accumulation was more pronounced than that induced by
497 100 nM BTZ, with previously reported LonP1 protease inhibition (IC_{50}=60 nM)[30]. BT317 also increased
498 Aco2 levels in an intracranial xenograft model. Further investigation of the role of Aco2 in malignant
499 astrocytoma metabolism and how the different BT317 moieties may enhance LonP1 protease inhibition
500 is warranted.

501 An important finding of our study is that the combination of BT317 and TMZ is more effective than BT317
502 or TMZ alone in IDH1-R132H GSC lines DB70 and DB76. The IDH wildtype GBM and astrocytoma cell lines
503 and the normal human fibroblast cell lines, HPF242 and MCF-10A, were less sensitive to combinatorial
504 treatment. Introduction of IDH1-R132H mutation to wildtype gliomas has been observed to increase ROS
505 generation[58] and decrease HIF1A[59-61] and NRF2 signaling[62]; however, this may be due to an altered hypoxic
506 response[63] and may also depend on the tumor microenvironment[59]. TMZ has been found to induce mTOR
507 signaling (e.g., pAKT)[64,65] and also subsequently block autophagy[65] in the 12-60 h range. This inhibition of
508 autophagy likely explains the strong synergy between TMZ and BT317, as BT317 clearly induces autophagy
509 and blocking autophagy with 3-MA was found to induce cell death. Additionally, the maximum tolerated
510 dose was exceptionally high, with little to no off-target proteasome inhibition. Targeting the GSC
511 population is critical for overcoming glioma treatment resistance. The dependence of GSCs on LonP1 and

512 CT-L proteasome activity is further highlighted by the upregulation of LonP1 in high-grade GSCs compared
513 to low-grade GSCs and neural stem cells (**Supplementary Fig. 2**). Proteasome activity also plays a key role
514 in cancer treatment resistance[25,26]. Interestingly, gliomas have elevated CT-L proteasome activity and,
515 generally, an increase in this activity serves as a compensatory response to prooxidative treatment[66].
516 Additional studies are vital to further explore the role of LonP1 and CT-L proteasome activity in malignant
517 glioma metabolism and whether dual inhibition could be useful for treating recurrent malignant
518 astrocytoma based on patient-specific genetic determinants. Future work will also seek to understand the
519 best route of administration, while also creating BT317 analogs that incorporate nanoparticles and other
520 moieties to optimize on-site and on-target activity to further the development of new therapeutic options
521 for malignant astrocytoma patients.

522 3. **References**

523 **1.** Ohgaki H, Dessen P, Jourde B, et al. Genetic Pathways to Glioblastoma: A Population-Based
524 Study. *Cancer research.* 2004; 64(19):6892-6899.
525 **2.** Sathornsumetee S, Rich JN, Reardon DA. Diagnosis and Treatment of High-Grade Astrocytoma.
526 *Neurologic Clinics.* 2007; 25(4):1111-1139.
527 **3.** Stupp R, Mason WP, van den Bent MJ, et al. Radiotherapy plus concomitant and adjuvant
528 temozolomide for glioblastoma. *N Engl J Med.* 2005; 352(10):987-996.
529 **4.** Rominiyi O, Vanderlinden A, Clenton SJ, Bridgewater C, Al-Tamimi Y, Collis SJ. Tumour treating
530 fields therapy for glioblastoma: current advances and future directions. *British Journal of Cancer.*
531 2021; 124(4):697-709.
532 **5.** Fisher JP, Adamson DC. Current FDA-Approved Therapies for High-Grade Malignant Gliomas.
533 *Biomedicines.* 2021; 9(3).
534 **6.** Hegi ME, Diserens AC, Gorlia T, et al. MGMT gene silencing and benefit from temozolomide in
535 glioblastoma. *N Engl J Med.* 2005; 352(10):997-1003.
536 **7.** Ohgaki H, Kleihues P. The definition of primary and secondary glioblastoma. *Clin Cancer Res.*
537 2013; 19(4):764-772.
538 **8.** Louis DN, Perry A, Wesseling P, et al. The 2021 WHO Classification of Tumors of the Central
539 Nervous System: a summary. *Neuro-Oncology.* 2021; 23(8):1231-1251.
540 **9.** Yan H, Parsons DW, Jin G, et al. IDH1 and IDH2 mutations in gliomas. *N Engl J Med.* 2009;
541 360(8):765-773.
542 **10.** Golub D, Iyengar N, Dogra S, et al. Mutant Isocitrate Dehydrogenase Inhibitors as Targeted
543 Cancer Therapeutics. *Front Oncol.* 2019; 9:417.
544 **11.** Liu Y, Lu Y, Celiku O, et al. Targeting IDH1-Mutated Malignancies with NRF2 Blockade. *J Natl*
545 *Cancer Inst.* 2019; 111(10):1033-1041.
546 **12.** Li Z, Bao S, Wu Q, et al. Hypoxia-inducible factors regulate tumorigenic capacity of glioma stem
547 cells. *Cancer Cell.* 2009; 15(6):501-513.
548 **13.** Gordan JD, Thompson CB, Simon MC. HIF and c-Myc: Sibling Rivals for Control of Cancer Cell
549 Metabolism and Proliferation. *Cancer Cell.* 2007; 12(2):108-113.
550 **14.** Forsythe JA, Jiang BH, Iyer NV, et al. Activation of vascular endothelial growth factor gene
551 transcription by hypoxia-inducible factor 1. *Molecular and Cellular Biology.* 1996; 16(9):4604-
552 4613.
553 **15.** Kaur B, Khwaja FW, Severson EA, Matheny SL, Brat DJ, Van Meir EG. Hypoxia and the hypoxia-
554 inducible-factor pathway in glioma growth and angiogenesis. *Neuro-oncology.* 2005; 7(2):134-
555 153.

556 **16.** Yang L, Lin C, Wang L, Guo H, Wang X. Hypoxia and hypoxia-inducible factors in glioblastoma
557 multiforme progression and therapeutic implications. *Experimental Cell Research.* 2012;
558 318(19):2417-2426.
559 **17.** Fukuda R, Zhang H, Kim JW, Shimoda L, Dang CV, Semenza GL. HIF-1 regulates cytochrome
560 oxidase subunits to optimize efficiency of respiration in hypoxic cells. *Cell.* 2007; 129(1):111-122.
561 **18.** Rep M, van Dijl JM, Suda K, Schatz G, Grivell LA, Suzuki CK. Promotion of mitochondrial
562 membrane complex assembly by a proteolytically inactive yeast Lon. *Science (New York, N.Y.).*
563 1996; 274(5284):103-106.
564 **19.** Liu T, Lu B, Lee I, Ondrovicova G, Kutejova E, Suzuki CK. DNA and RNA binding by the
565 mitochondrial lon protease is regulated by nucleotide and protein substrate. *The Journal of*
566 *biological chemistry.* 2004; 279(14):13902-13910.
567 **20.** Quiros PM, Espanol Y, Acin-Perez R, et al. ATP-dependent Lon protease controls tumor
568 bioenergetics by reprogramming mitochondrial activity. *Cell Rep.* 2014; 8(2):542-556.
569 **21.** Cheng CW, Kuo CY, Fan CC, et al. Overexpression of Lon contributes to survival and aggressive
570 phenotype of cancer cells through mitochondrial complex I-mediated generation of reactive
571 oxygen species. *Cell Death Dis.* 2013; 4:e681.
572 **22.** Di K, Lomeli N, Wood SD, Vanderwal CD, Bota DA. Mitochondrial Lon is over-expressed in high-
573 grade gliomas, and mediates hypoxic adaptation: potential role of Lon as a therapeutic target in
574 glioma. *Oncotarget.* 2016; 7(47):77457-77467.
575 **23.** Bayot A, Basse N, Lee I, et al. Towards the control of intracellular protein turnover:
576 Mitochondrial Lon protease inhibitors versus proteasome inhibitors. *Biochimie.* 2008; 90(2):260-
577 269.
578 **24.** Stahlberg H, Kutejová E, Suda K, et al. Mitochondrial Lon of Saccharomyces
579 cerevisiae is a ring-shaped protease with seven flexible subunits. *Proceedings of the*
580 *National Academy of Sciences.* 1999; 96(12):6787-6790.
581 **25.** Adams J. The proteasome: structure, function, and role in the cell. *Cancer Treat Rev.* 2003; 29
582 Suppl 1:3-9.
583 **26.** Patel NM, Nozaki S, Shortle NH, et al. Paclitaxel sensitivity of breast cancer cells with
584 constitutively active NF-kappaB is enhanced by IkappaBalpha super-repressor and parthenolide.
585 *Oncogene.* 2000; 19(36):4159-4169.
586 **27.** Maneix L, Sweeney MA, Lee S, et al. The Mitochondrial Protease LonP1 Promotes Proteasome
587 Inhibitor Resistance in Multiple Myeloma. *Cancers (Basel).* 2021; 13(4).
588 **28.** Lee J, Pandey AK, Venkatesh S, et al. Inhibition of mitochondrial LonP1 protease by allosteric
589 blockade of ATP binding and hydrolysis via CDDO and its derivatives. *The Journal of biological*
590 *chemistry.* 2022; 298(3):101719.
591 **29.** Gibellini L, Pinti M, Bartolomeo R, et al. Inhibition of Lon protease by triterpenoids alters
592 mitochondria and is associated to cell death in human cancer cells. *Oncotarget.* 2015;
593 6(28):25466-25483.
594 **30.** Csizmadia V, Hales P, Tsu C, et al. Proteasome inhibitors bortezomib and carfilzomib used for the
595 treatment of multiple myeloma do not inhibit the serine protease HtrA2/Omi. *Toxicol Res*
596 *(Camb).* 2016; 5(6):1619-1628.
597 **31.** Takeshima K, Mizuno K, Nakahashi H, Aoki H, Kanekiyo Y. Ratiometric Sensing of Hydrogen
598 Peroxide Utilizing Conformational Change in Fluorescent Boronic Acid Polymers. *Journal of*
599 *Analytical Methods in Chemistry.* 2017; 2017:7829438.
600 **32.** Huehnchen P, Springer A, Kern J, et al. Bortezomib at therapeutic doses poorly passes the
601 blood–brain barrier and does not impair cognition. *Brain Communications.* 2020; 2(1).

602 **33.** Tang JH, Yang L, Chen JX, et al. Bortezomib inhibits growth and sensitizes glioma to
603 temozolomide (TMZ) via down-regulating the FOXM1-Survivin axis. *Cancer Commun (Lond).*
604 2019; 39(1):81.
605 **34.** Seidel S, Garvalov BK, Acker T. Isolation and Culture of Primary Glioblastoma Cells from Human
606 Tumor Specimens. In: Rich IN, ed. *Stem Cell Protocols*. New York, NY: Springer New York;
607 2015:263-275.
608 **35.** Van der Borght K, Tourny A, Bagdziunas R, et al. BIGL: Biochemically Intuitive Generalized Loewe
609 null model for prediction of the expected combined effect compatible with partial agonism and
610 antagonism. *Sci Rep.* 2017; 7(1):17935.
611 **36.** Aston WJ, Hope DE, Nowak AK, Robinson BW, Lake RA, Lesterhuis WJ. A systematic investigation
612 of the maximum tolerated dose of cytotoxic chemotherapy with and without supportive care in
613 mice. *BMC cancer.* 2017; 17(1):684-684.
614 **37.** Hubert CG, Rivera M, Spangler LC, et al. A Three-Dimensional Organoid Culture System Derived
615 from Human Glioblastomas Recapitulates the Hypoxic Gradients and Cancer Stem Cell
616 Heterogeneity of Tumors Found In Vivo. *Cancer research.* 2016; 76(8):2465-2477.
617 **38.** Mizushima N, Yoshimori T. How to interpret LC3 immunoblotting. *Autophagy.* 2007; 3(6):542-
618 545.
619 **39.** Vassallo JD, Hicks SM, Daston GP, Lehman-McKeeman LD. Metabolic Detoxification Determines
620 Species Differences in Coumarin-Induced Hepatotoxicity. *Toxicological Sciences.* 2004;
621 80(2):249-257.
622 **40.** Lassalas P, Gay B, Lasfargeas C, et al. Structure Property Relationships of Carboxylic Acid
623 Isosteres. *Journal of medicinal chemistry.* 2016; 59(7):3183-3203.
624 **41.** Halasi M, Wang M, Chavan Tanmay S, Gaponenko V, Hay N, Gartel Andrei L. ROS inhibitor N-
625 acetyl-L-cysteine antagonizes the activity of proteasome inhibitors. *Biochemical Journal.* 2013;
626 454(2):201-208.
627 **42.** Manton CA, Johnson B, Singh M, Bailey CP, Bouchier-Hayes L, Chandra J. Induction of cell death
628 by the novel proteasome inhibitor marizomib in glioblastoma in vitro and in vivo. *Scientific*
629 *Reports.* 2016; 6(1):18953.
630 **43.** Bota DA, Davies KJ. Lon protease preferentially degrades oxidized mitochondrial aconitase by an
631 ATP-stimulated mechanism. *Nature cell biology.* 2002; 4(9):674-680.
632 **44.** Chen J, Li Y, Yu T-S, et al. A restricted cell population propagates glioblastoma growth after
633 chemotherapy. *Nature.* 2012; 488(7412):522-526.
634 **45.** Vik-Mo EO, Sandberg C, Olstorn H, et al. Brain tumor stem cells maintain overall phenotype and
635 tumorigenicity after in vitro culturing in serum-free conditions. *Neuro Oncol.* 2010; 12(12):1220-
636 1230.
637 **46.** Gong X, Schwartz PH, Linskey ME, Bota DA. Neural stem/progenitors and glioma stem-like cells
638 have differential sensitivity to chemotherapy. *Neurology.* 2011; 76(13):1126-1134.
639 **47.** Ferretti M, Fabbiano C, Di Bari M, et al. M2 receptor activation inhibits cell cycle progression and
640 survival in human glioblastoma cells. *Journal of cellular and molecular medicine.* 2013; 17.
641 **48.** Di K, Lloyd GK, Abraham V, et al. Marizomib activity as a single agent in malignant gliomas:
642 ability to cross the blood-brain barrier. *Neuro-oncology.* 2016; 18(6):840-848.
643 **49.** Rutkowski S, Gerber NU, von Hoff K, et al. Treatment of early childhood medulloblastoma by
644 postoperative chemotherapy and deferred radiotherapy. *Neuro-Oncology.* 2009; 11(2):201-210.
645 **50.** Velasco R, Alberti P, Bruna J, Psimaras D, Argyriou AA. Bortezomib and other proteosome
646 inhibitors—induced peripheral neurotoxicity: From pathogenesis to treatment. *Journal of the*
647 *Peripheral Nervous System.* 2019; 24(S2):S52-S62.
648 **51.** Roth P, Gorlia T, Reijneveld JC, et al. EORTC 1709/CCTG CE.8: A phase III trial of marizomib in
649 combination with temozolomide-based radiochemotherapy versus temozolomide-based

650 radiochemotherapy alone in patients with newly diagnosed glioblastoma. Paper presented at:
651 ASCO Annual Meeting2021.
652 **52.** Lovering F, Bikker J, Humblet C. Escape from flatland: increasing saturation as an approach to
653 improving clinical success. *Journal of medicinal chemistry.* 2009; 52(21):6752-6756.
654 **53.** Bota DA, Eroglu Z, Reardon DA, et al. Phase II clinical trial of bortezomib and bevacizumab
655 combination in recurrent glioblastoma. *Journal of Clinical Oncology.* 2011; 29(15_suppl):2056-
656 2056.
657 **54.** Laurent N, de Boüard S, Guillamo JS, et al. Effects of the proteasome inhibitor ritonavir on
658 glioma growth in vitro and in vivo. *Mol Cancer Ther.* 2004; 3(2):129-136.
659 **55.** Bota DA, Mason W, Kesari S, et al. Marizomib alone or in combination with bevacizumab in
660 patients with recurrent glioblastoma: Phase I/II clinical trial data. *Neurooncol Adv.* 2021;
661 3(1):vdab142-vdab142.
662 **56.** Ciccarone F, Di Leo L, Lazzarino G, et al. Aconitase 2 inhibits the proliferation of MCF-7 cells
663 promoting mitochondrial oxidative metabolism and ROS/FoxO1-mediated autophagic response.
664 *British Journal of Cancer.* 2020; 122(2):182-193.
665 **57.** Farooq MA, Pracheil TM, Dong Z, Xiao F, Liu Z. Mitochondrial DNA Instability in Cells Lacking
666 Aconitase Correlates with Iron Citrate Toxicity. *Oxidative Medicine and Cellular Longevity.* 2013;
667 2013:493536.
668 **58.** Li LC, Zhang M, Feng YK, Wang XJ. IDH1-R132H Suppresses Glioblastoma Malignancy through
669 FAT1-ROS-HIF-1α Signaling. *Neurol India.* 2020; 68(5):1050-1058.
670 **59.** Williams SC, Karajannis MA, Chiriboga L, Golfinos JG, von Deimling A, Zagzag D. R132H-mutation
671 of isocitrate dehydrogenase-1 is not sufficient for HIF-1α upregulation in adult glioma. *Acta*
672 *Neuropathol.* 2011; 121(2):279-281.
673 **60.** Yao J, Chakhoyan A, Nathanson DA, et al. Metabolic characterization of human IDH mutant and
674 wild type gliomas using simultaneous pH- and oxygen-sensitive molecular MRI. *Neuro-Oncology.*
675 2019; 21(9):1184-1196.
676 **61.** Xu W, Yang H, Liu Y, et al. Oncometabolite 2-Hydroxyglutarate Is a Competitive Inhibitor of α-
677 Ketoglutarate-Dependent Dioxygenases. *Cancer Cell.* 2011; 19(1):17-30.
678 **62.** Li K, Ouyang L, He M, et al. IDH1 R132H mutation regulates glioma chemosensitivity through
679 Nrf2 pathway. *Oncotarget.* 2017; 8(17):28865-28879.
680 **63.** Dao Trong P, Rösch S, Mairbäurl H, et al. Identification of a Prognostic Hypoxia-Associated Gene
681 Set in IDH-Mutant Glioma. *Int J Mol Sci.* 2018; 19(10).
682 **64.** Murphy SF, Varghese RT, Lamouille S, et al. Connexin 43 Inhibition Sensitizes Chemoresistant
683 Glioblastoma Cells to Temozolomide. *Cancer research.* 2016; 76(1):139-149.
684 **65.** Yu Z, Zhao G, Xie G, et al. Metformin and temozolomide act synergistically to inhibit growth of
685 glioma cells and glioma stem cells in vitro and in vivo. *Oncotarget.* 2015; 6(32):32930-32943.
686 **66.** Kretz-Remy C, Arrigo A-P. Modulation of the chymotrypsin-like activity of the 20S proteasome
687 by intracellular redox status: effects of glutathione peroxidase-1 overexpression and antioxidant
688 drugs. *Biol Chem.* 2003; 384(4):589-595.

689

690

691

Graphical Abstract. BT317, a novel dual Chymotrypsin-like proteasome and LonP1 inhibitor drives autophagy-dependent cell death and exhibits synergy with TMZ through induction of the mTOR signaling pathway

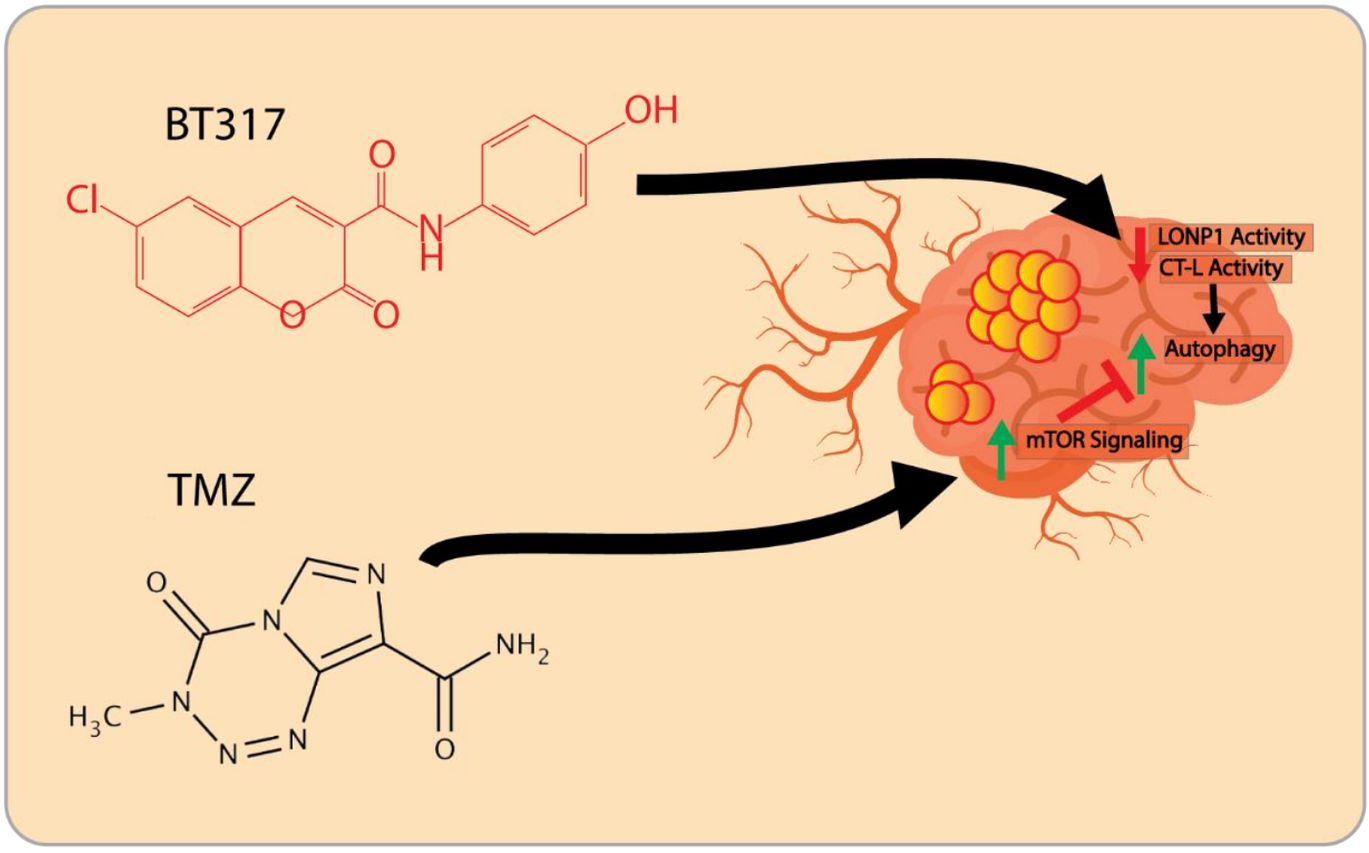

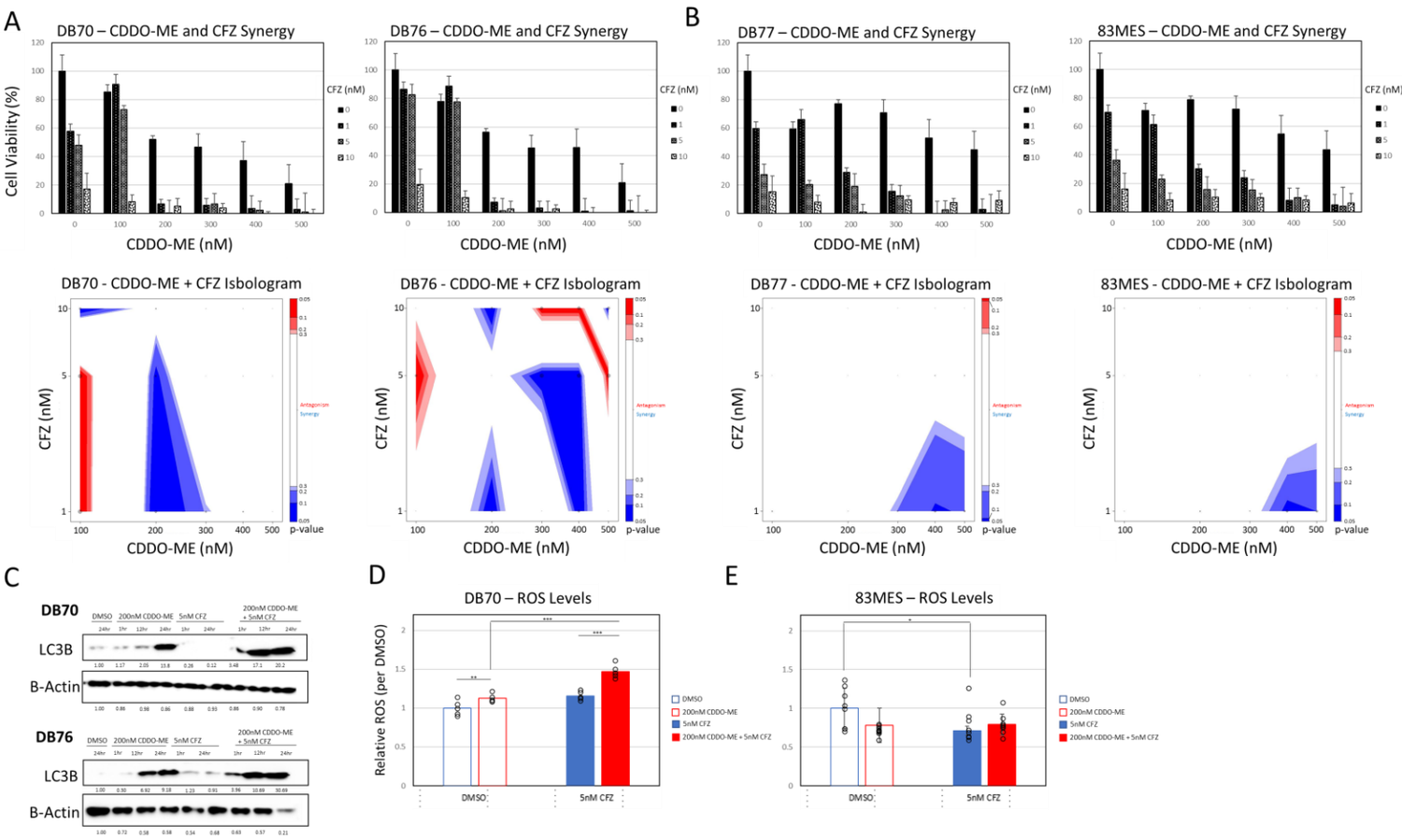

Figure 1. Dual LonP1 and Chymotrypsin-like Proteasome Inhibition has Greater Synergy in IDH1 Mutant Astrocytoma and Enhances Autophagy and ROS Production. (**A**) In combination with Carfilzomib, a selective chymotrypsin-like proteasome inhibitor, CDDO-ME, a known LonP1 inhibitor, demonstrates strong synergy at 200nM in IDH1 mutant lines, whereas (B) the IDH1 wildtype lines only show limited synergy at 400-500nM. (C) Lc3B levels and (D) ROS levels were assessed after the combination of 5nM CFZ and 200nM CDDO-ME at 1, 12 and 24 hour timepoints in the DB70 and DB76 lines. (E) Similarly ROS levels were analyzed in the 83MES line. Statistical significance was determined by t-test. * P <0.05, ** P <0.01, *** P <0.001; n.s., not significant.

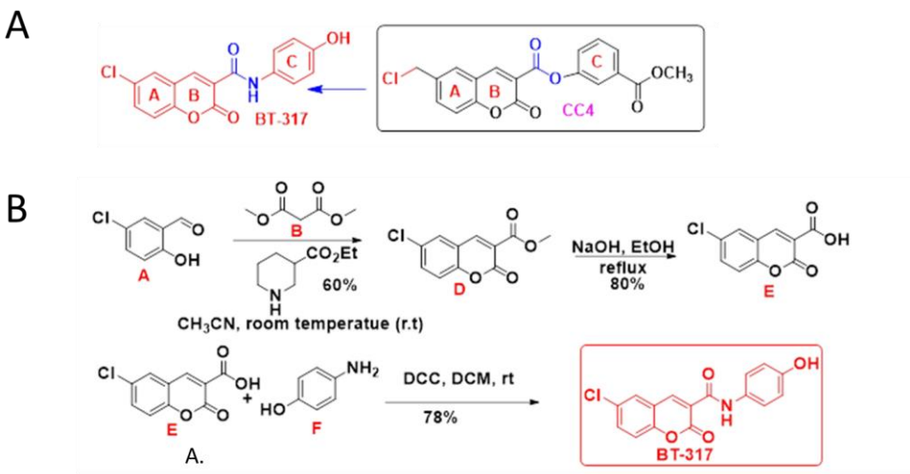

Figure 2. LonP1 small molecule inhibitor BT317 was derived from CC4. (**A**) BT317 is an analog of CC4. (**B**) Synthesis of BT317.

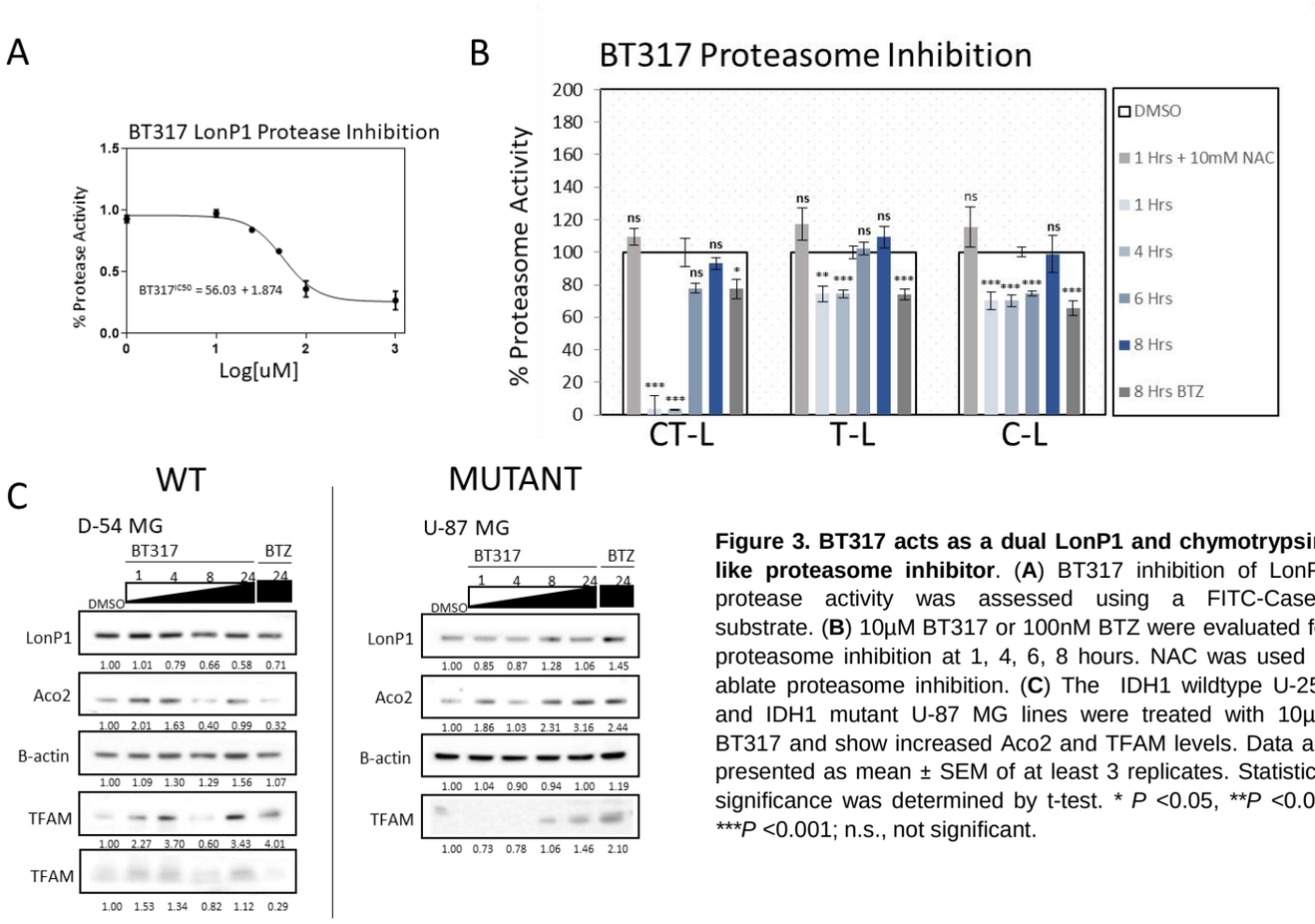

Figure 3. BT317 acts as a dual LonP1 and chymotrypsin-like proteasome inhibitor. (**A**) BT317 inhibition of LonP1 protease activity was assessed using a FITC-Casein substrate. (**B**) 10µM BT317 or 100nM BTZ were evaluated for proteasome inhibition at 1, 4, 6, 8 hours. NAC was used to ablate proteasome inhibition. (**C**) The IDH1 wildtype U-251 and IDH1 mutant U-87 MG lines were treated with 10µM BT317 and show increased Aco2 and TFAM levels. Data are presented as mean ± SEM of at least 3 replicates. Statistical significance was determined by t-test. * P <0.05, ** P <0.01, *** P <0.001; n.s., not significant.

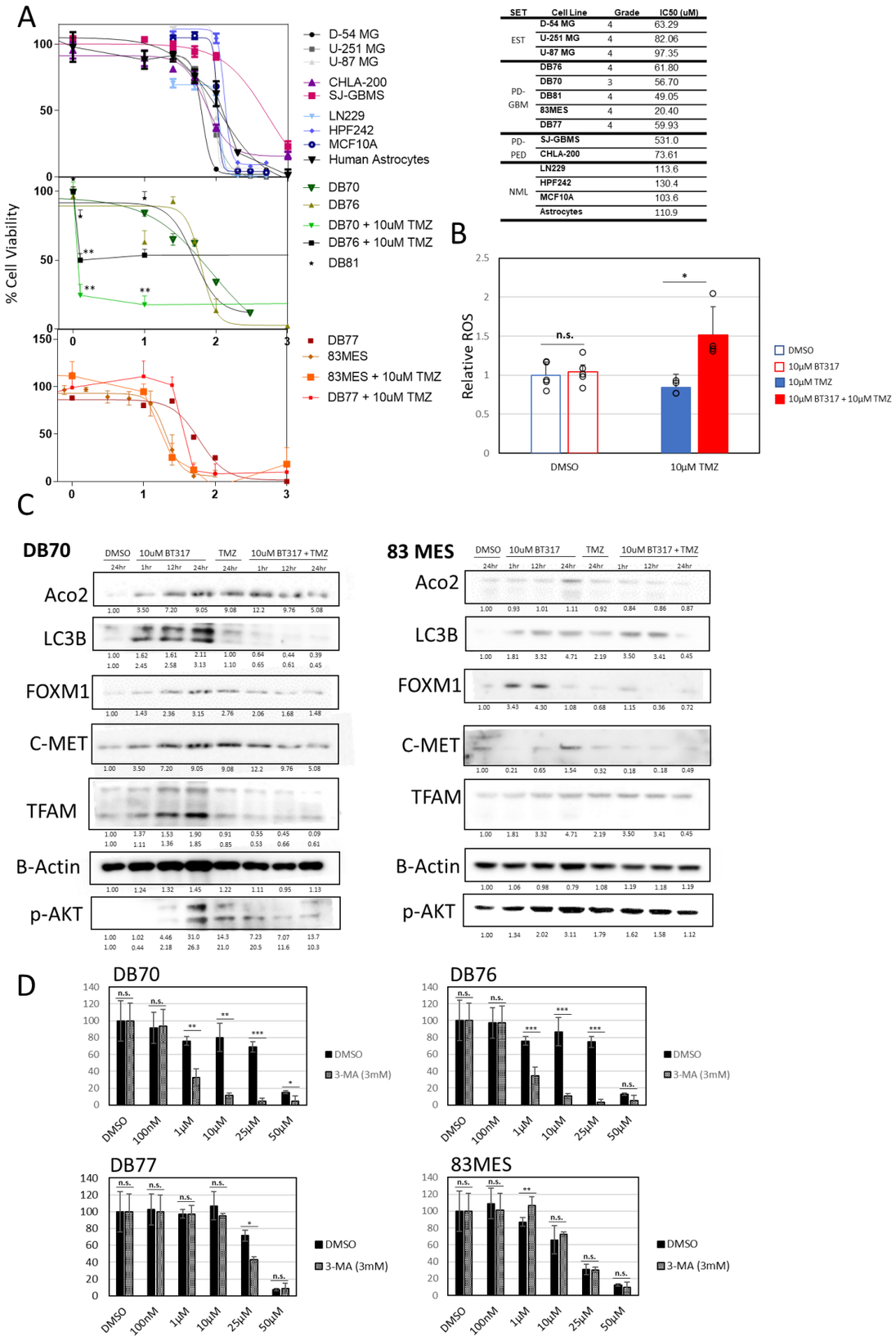

SET	Cell Line	Grade	IC50 (uM)
EST	D-54 MG	4	63.29
	U-251 MG	4	82.06
	U-87 MG	4	97.35
PD-GBM	DB76	4	61.80
	DB70	3	56.70
	DB81	4	49.05
	83MES	4	20.40
	DB77	4	59.93
PD-PED	SJ-GBMS		531.0
	CHLA-200		73.61
NML	LN229		113.6
	HPF242		130.4
	MCF10A		103.6
	Astrocytes		110.9

Figure 4. BT317 drives autophagy-dependent cell death in specifically IDH1 mutant astrocytoma and TMZ works synergistically by blocking autophagy. (A) human neural stem cells (do you have data on NSC? Please include), astrocytes, multiple fibroblast lines), established GBM lines (panel 1), IDH1 mutant glioma lines DB70 and DB76 ± 10μM TMZ (panel 2), and IDH1 wildtype glioma lines DB77 and 83MES ± 10μM TMZ (panel 3) were treated with titrated doses of BT317 for 5 days prior to measuring viability. (B) ROS were measured using CellROX Orange at 12 hours and (C) protein samples analyzed following incubation with 10μM BT317 ± 10μM TMZ at 1, 12 and 24 hours as detailed. (D) The IDH1 mutant and wildtype lines were analyzed for autophagy-dependent cell death following titer of BT317 and co-incubation with 3mM 3-MA for 5 days. Statistical significance was determined by t-test. * P <0.05, ** P <0.01, *** P <0.001; n.s., not significant.

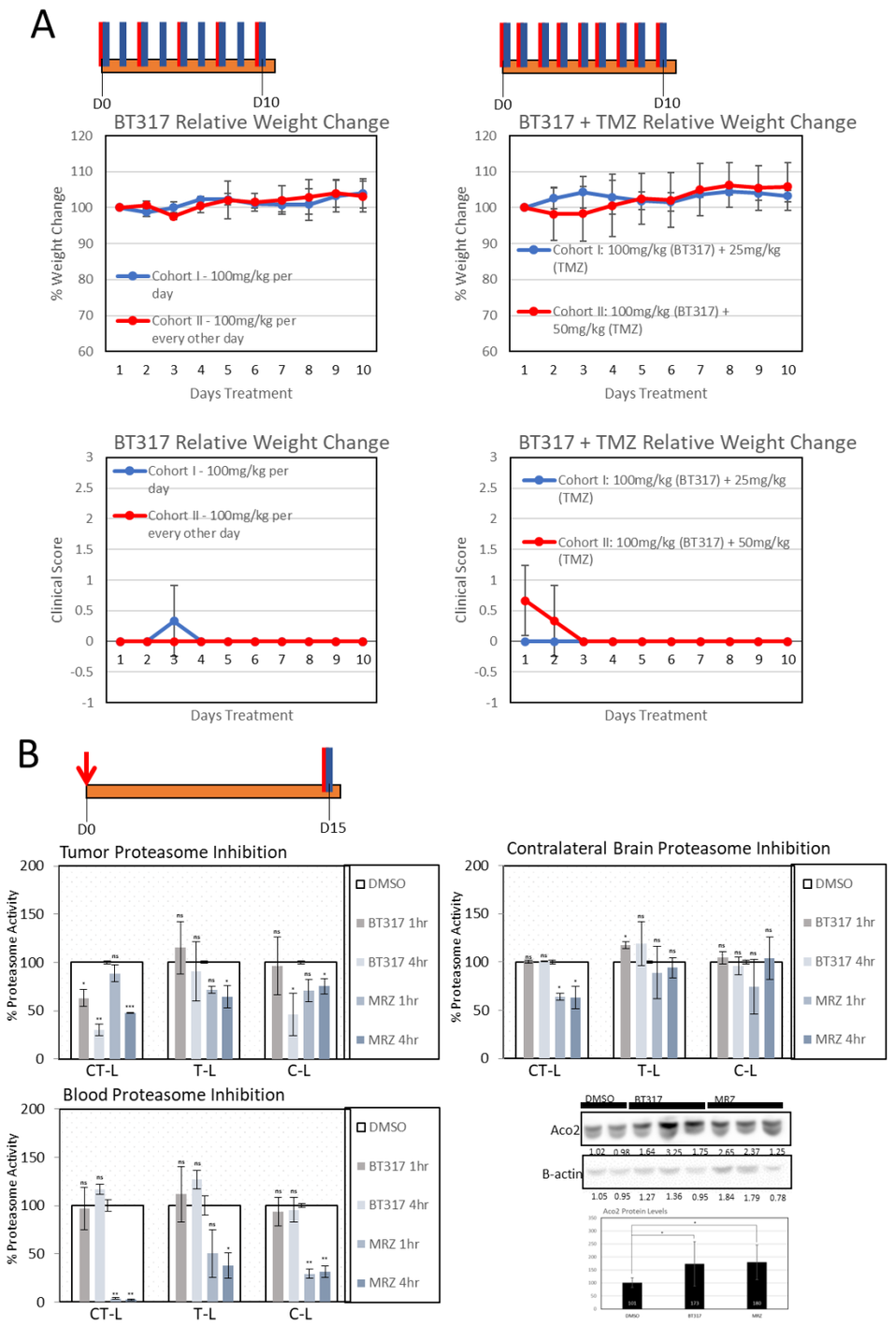

Figure 5. The combination of BT317 and TMZ has minimal toxicity in NSG mice. (**A**) BT317 was administered at 100mg/kg every other or every day for 10 total days ± 25 or 50 mg/kg TMZ and weight and clinical score was monitored. (**B**) 15 days after intracranial implantation of DB70, BT317 (100mg/kg), Marizomib (50µg/kg) or DMSO (w/v) were injected i.p. at various doses to proteasome activity and Aco2 levels in the tumor, healthy brain and blood at 1 and 4 hours. Statistical significance was determined by t-test. * P <0.05, ** P <0.01, *** P <0.001; n.s., not significant.

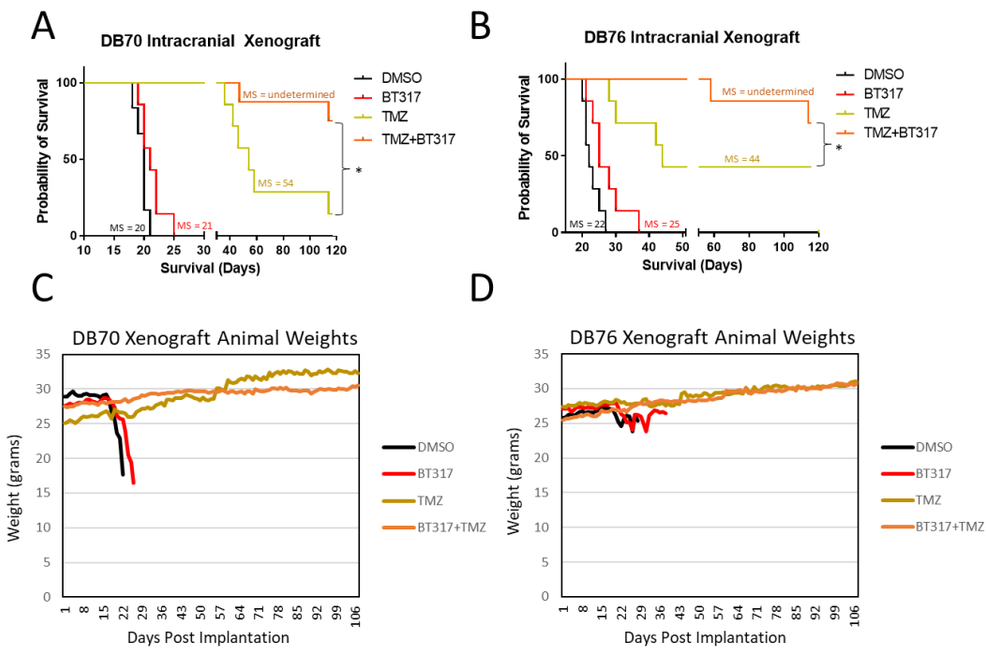

Figure 6. BT317 and Combinatorial BT317 + TMZ Treatment Significantly Improves Survival. (**A**) In the DB70 intracranial model, 100 mg/kg BT317 ± 100 mg/kg TMZ was injected i.p. daily for 5 days starting on day 10 after intracranial implantation. (**B**) The methodology in (A) was applied to assess any survival advantage in the DB76 intracranial xenograft model. Average weights of animals were tracked from post-implantation for (C) DB70 and (D) DB76. Significance was measured n=3 per endpoint).;*p<0.05, **p<0.01, ***p<0.001 ns=not significant. (BT317, n=6; MRZ, n=6, DMSO n=4 per endpoint).

Patient-derived GSC Lines					
Line	Classification	Grade	IDH1	p53	ATRX
DB70	Astrocytoma	3	Mut	Lost	Lost
DB76	Astrocytoma	4	Mut	Lost	Lost
DB77	Astrocytoma	4	WT	WT	WT
83MES	Glioblastoma	4	WT	N/A	N/A
DB81	Astrocytoma	4	Mut	Lost	Lost

Table 1. Lines for patient-derived samples included in this study.

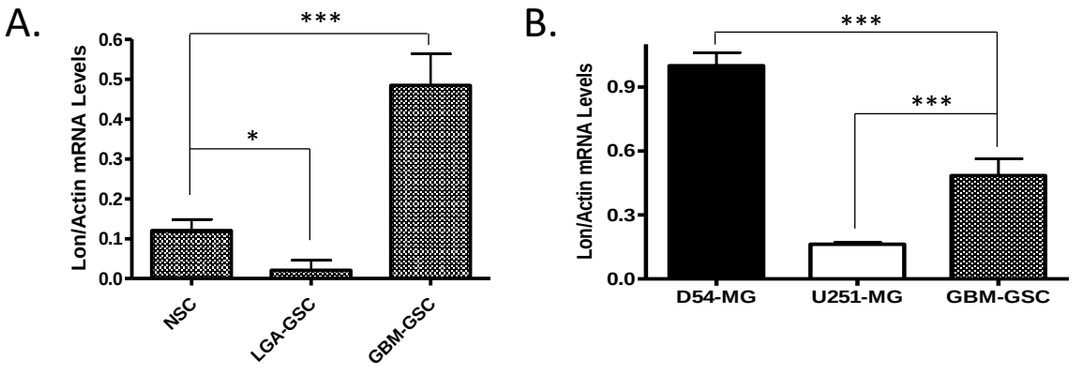

Supplementary Figure S1. LonP1 expression is upregulated in late-stage GBM. (**A**) LonP1 levels were normalized to B-actin via qtPCR for neural stem cells (NSC), low-grade glioma stem cells (LGA-GSC) and glioblastoma glioma stem cells (GBM-GSC). (**B**) Similarly, LonP1 levels were assessed to determine expression in the established D-54 MG, U-251 MG and GBM-GSC lines.

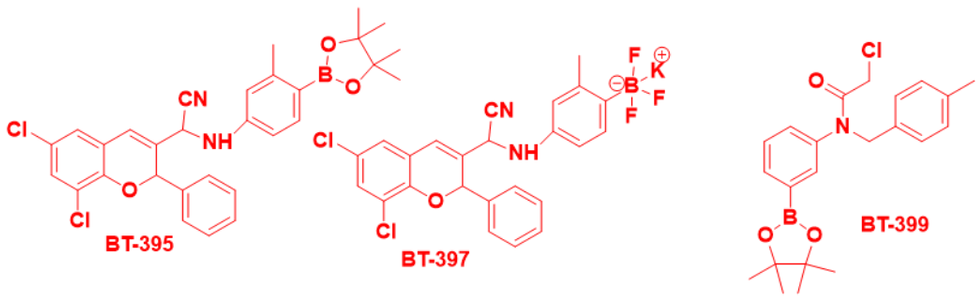

Supplementary Figure S2. CC4 was also used to derive BT395, BT397 and BT399. Chemical structures are as shown.

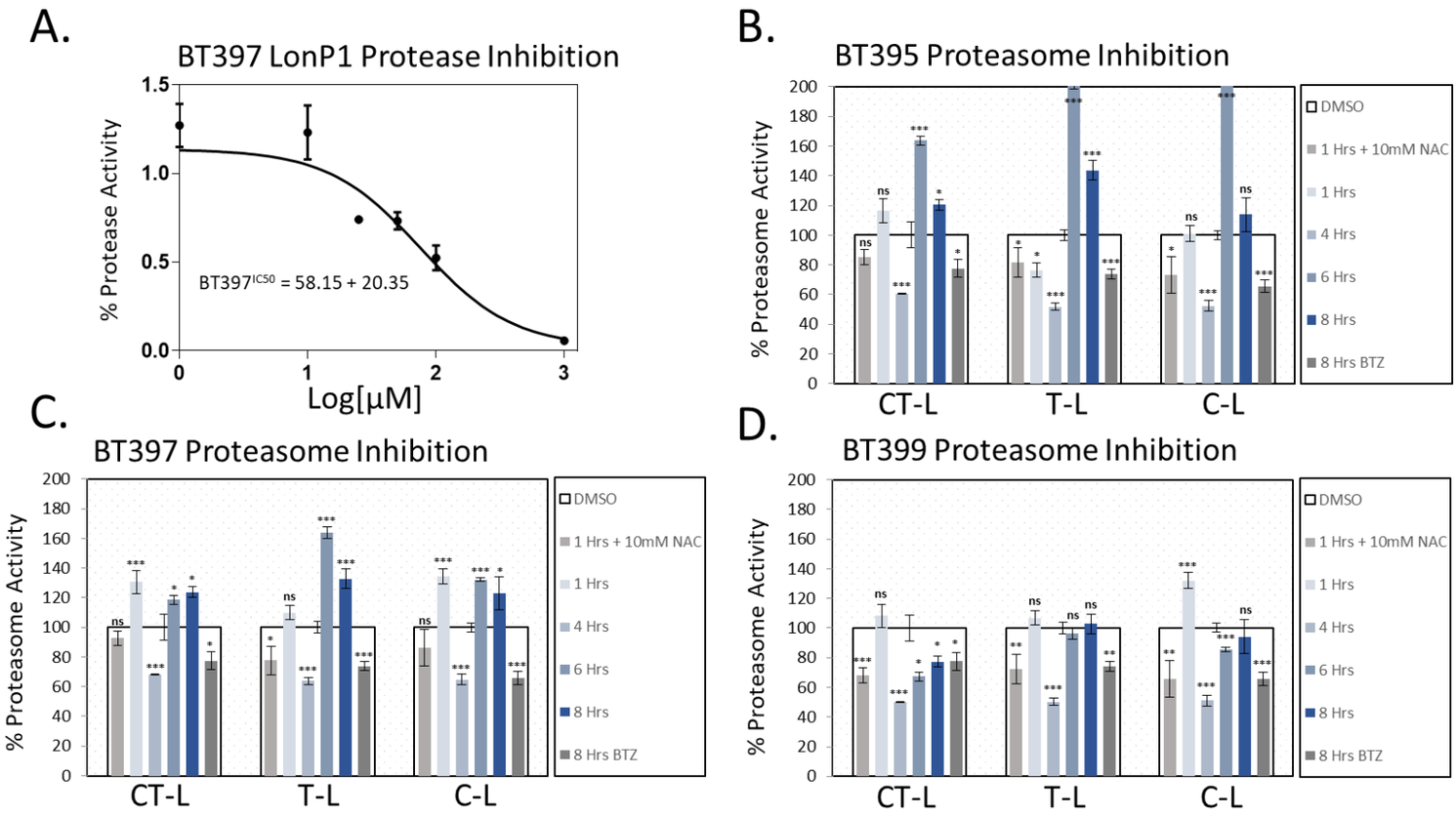

Supplementary Figure S3. BT395, BT397 and BT399 Show Limited Inhibition of LonP1 and Proteasome Activity. (**A**) BT397 was assessed for inhibition of LonP1 protease activity with an IC50 established at 58.15µM (**B-D**) BT395, BT397 and BT399 have variable levels of short-term proteasome inhibition. NAC= N-acetyl Cysteine; BTZ = Bortezomib; CT-L= Chymotrypsin-like activity; T-L = Trypsin-like activity; C-L = Caspase-like activity. Statistical significance was determined by t-test. * P <0.05, **P <0.01, ***P <0.001; n.s., not significant.

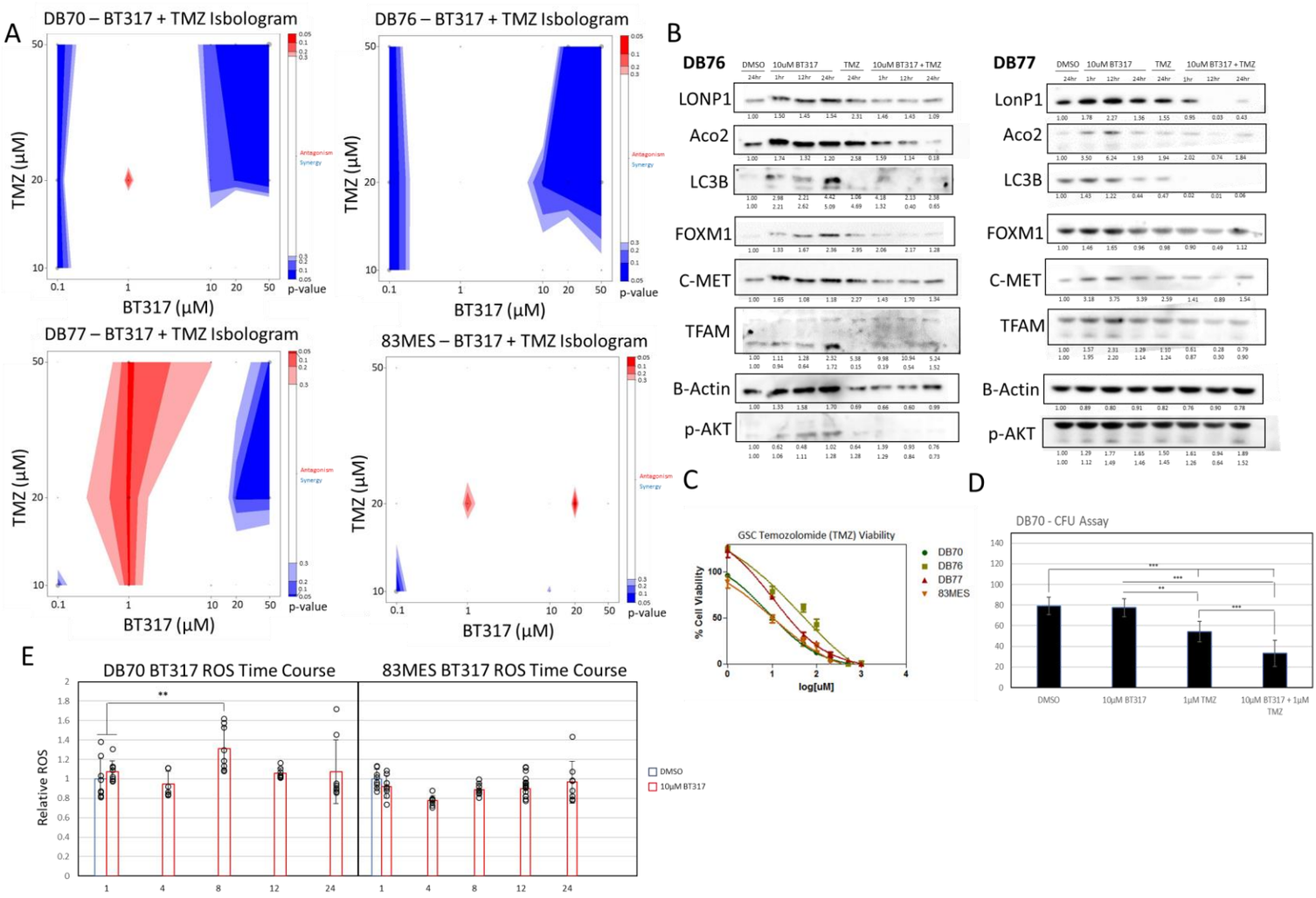

Supplementary Figure S4. BT317 Shows Strong Synergy with TMZ in IDH Mutant GSC Lines. (**A**) Synergy between BT317 and TMZ was evaluated using BIG, with blue representing significant synergy and red representing anergy. (**B**) Protein levels were evaluated at 10μM BT317 ± 10μM TMZ for 1-24 hours. (C) Relative sensitivity of each GSC line to TMZ. (D) The DB70 line was subjected to 10μM BT317 ± 10μM TMZ for 24 hours and evaluated for colony forming ability 12 days later. (E) ROS levels were analyzed following BT317 treatment at 1, 4, 9, 12 and 24 hours. Statistical significance was determined by t-test. * P <0.05, **P <0.01, ***P <0.001; n.s., not significant.

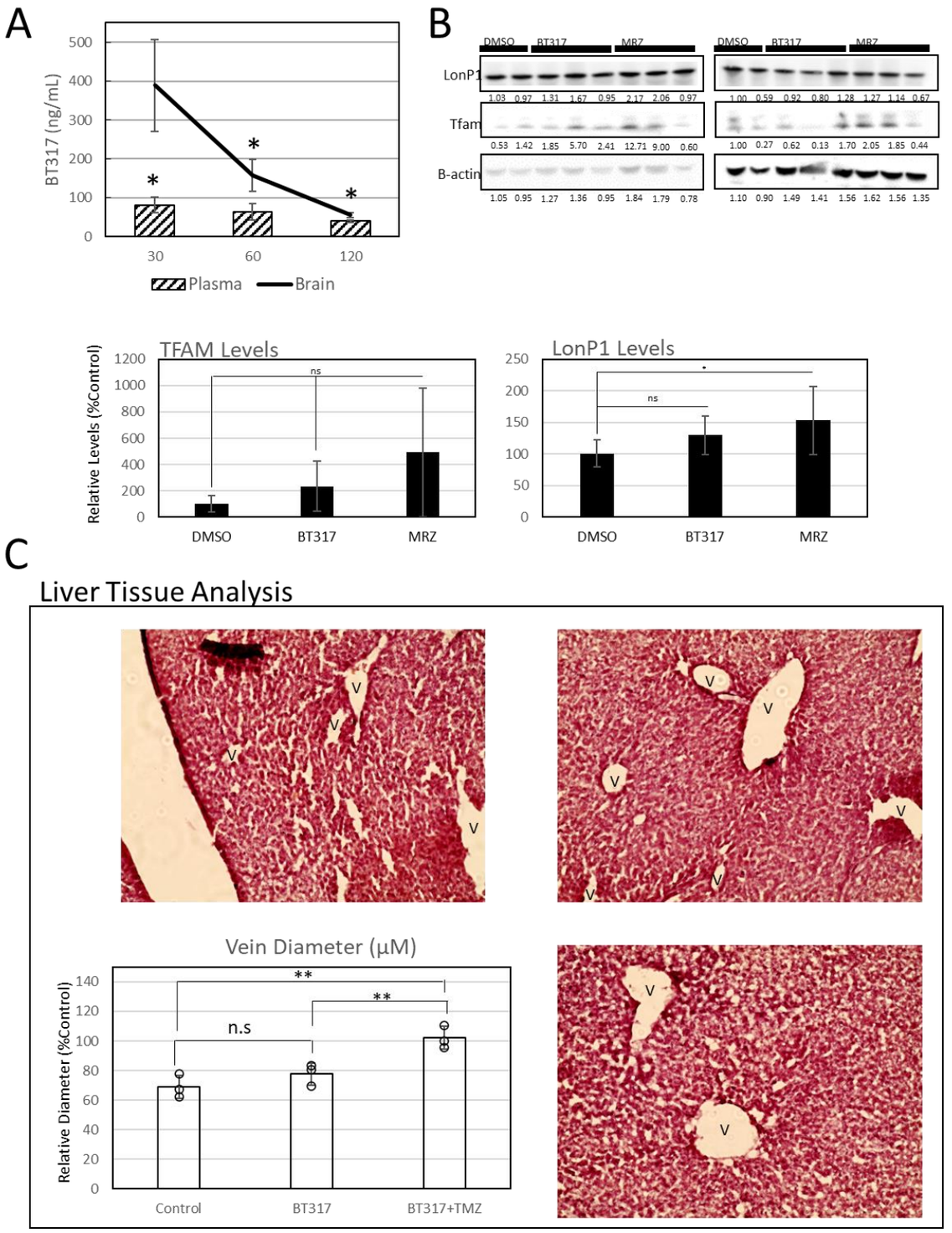

Supplementary Figure S5. BT317 Shows BBB Permeability, Increased LonP1 Inhibition in the Tumor Xenograft and Limited Liver Toxicity . (**A**) Following i.p. injection of 3mg/kg BT317, blood and brain samples were assessed via LC-MS for compound levels. (**B**) Protein levels were evaluated following injection of 100mg/kg of BT317 and 15 days post intracranial xenograft implantation. (**C**) Liver toxicity was evaluated for gross morphological differences and vein diameter following 100mg/kg of BT317 administered daily for 10 days total. Statistical significance was determined by t-test. * P <0.05, **P <0.01, ***P <0.001; n.s., not significant.

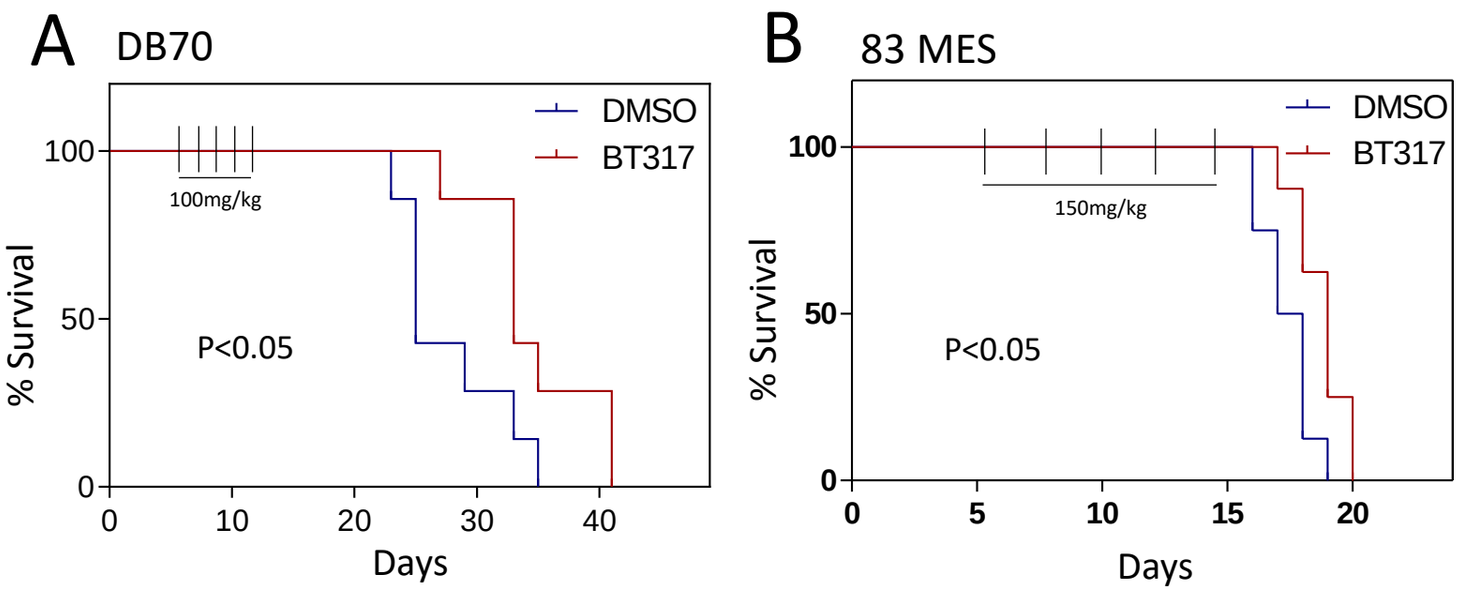

Supplementary Figure S6. BT317 Shows Efficacy Against the 83MES GSC Line. (A) 100 mg/kg in the DB70 or (B) 150 mg/kg BT317 in the 83MES xenograft model was injected i.p. every other day for 5 total doses starting on day 5 after intracranial implantation**.** Significance was measured n=7 per endpoint).;*p<0.05, **p<0.01, ***p<0.001 ns=not significant. (BT317, n=6; MRZ, n=6, DMSO n=4 per endpoint).